DAE- BRNS sponsored Theme Meeting on

Application of Molecular Modeling in Separation Processes

AMMSP2015

On

January 16, 2015

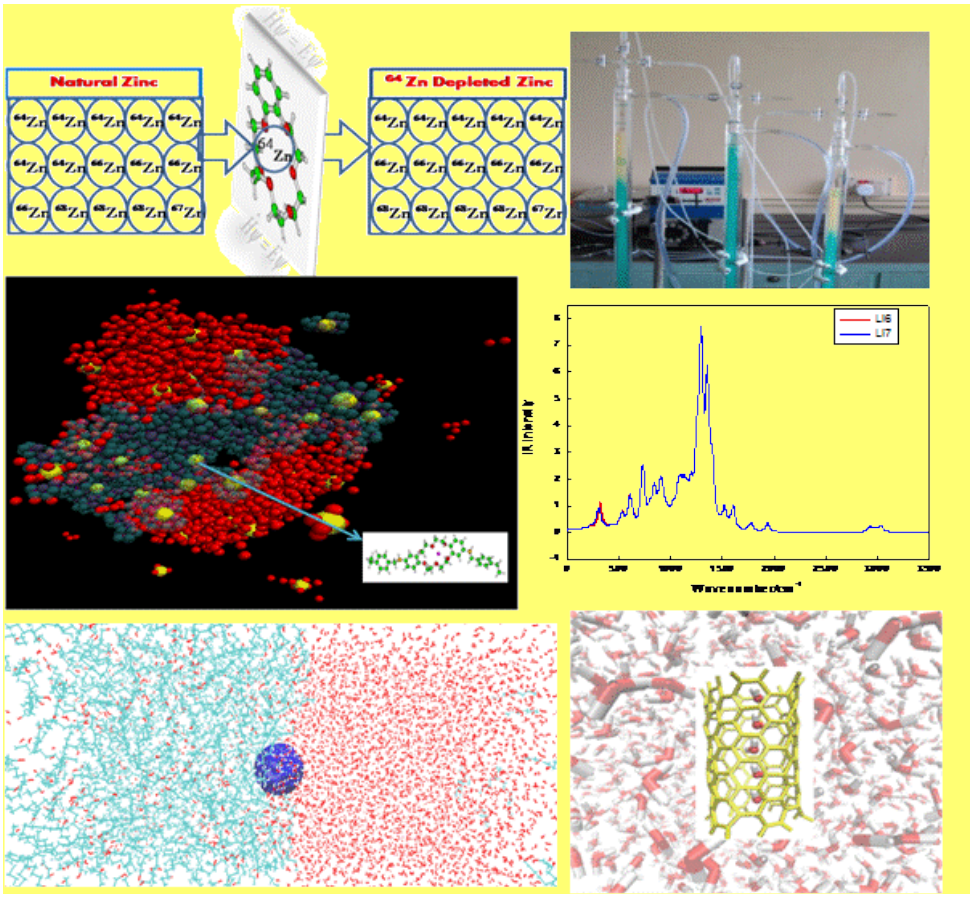

Venue:
C Block Auditorium, Mod Lab
Bhabha Atomic Research Centre

Organized By:
Chemical Engineering Division
Bhabha Atomic research Centre
Trombay, Mumbai – 400085

DAE- BRNS sponsored Theme Meeting on

Application of Molecular Modeling in Separation Processes

On

January 16, 2015

Bhabha Atomic Research Centre, Trombay, Mumbai – 400085

Organizing Committee

Advisory committee

P.K. Wattal (Chairman)
K.L. Ramakumar
P.K. Tiwari,
B.N. Jagatap
S.K. Sarkar
S.B. Roy
S. Mohan
R.S. Mundada
B. S. Tomar
A. K. Goswami
K.T. Shenoy
V.G. Gaikar
K.G. Ayappa
G.N. Sastry
J.K. Singh
Sangeeta

Organizing Committee

K.T. Shenoy (Convener)
K. K. Singh (Joint secretary)
S. Mukhopadhyay
D. Mandal
M.Y. Walke
N.K. Dandekar
S. Manivannan
N. A. Baveja
C.P. Shringi
K.N. Maithania
S. K. Arora
G. Varshney
Sangeeta Pal
Rajesh Kumar

Sk. M. Ali (Secretary)
J. M. Joshi (Treasurer)
S. Mishra
D. Thomas
A. Boda
S. Bhowmick
A. K. Singha Deb
N. Sen
M. Darekar
G. Pandey
P. Sahu
G. Nagesh
K. Bhatt
K. Vaibhav

Srikumar Banerjee
DAE Homi Bhabha Chair Professor

MESSAGE

December 31, 2014

Molecular modeling is becoming an increasingly important part of chemical research and education as computers become faster and programs become easier to use. Molecular modelling aims at understanding and designing of novel molecules and materials in the field of chemistry, material science, physics, chemical engineering, separation science, medical science, bioscience, etc. It provides valuable information particularly in situations with extreme conditions where experiments cannot be performed.

I am delighted to know that one day theme meeting on "Application of Molecular Modeling in Separation Processes" (AMMSP-2015) is being organized by Chemical Engineering Division, BARC, Mumbai on 16th January 2015.

I congratulate the organizers for planning this theme meeting which will help in further advancement of this thrust area of research. I am sure the present theme meeting will provide a platform for having close and fruitful interactions of various experimental and theoretical research groups of BARC and other premier institutes of the country. This is expected to generate new ideas and will give the young researchers an opportunity to formulate their research in the frontier area of separation science.

I wish the theme meeting all success.

Srikumar Banerjee

(Srikumar Banerjee)

4th Floor, Central Complex, Bhabha Atomic Research Centre, Trombay, Mumbai – 400 085
Tel.: 022-25505333 • Fax: 022-25505333 • E-mail: sbanerjee@barc.gov.in

शेखर बसु
Sekhar Basu

भारत सरकार
Government of India

निदेशक, भाभा परमाणु अनुसंधान केंद्र
Director, Bhabha Atomic Research Centre
सदस्य, परमाणु ऊर्जा आयोग
Member, Atomic Energy Commission

MESSAGE

I am glad to know that the theme meeting on "Application of Molecular Modeling in Separation Processes" (AMMSP-2015) is being organised by Chemical Engineering Division, BARC, Mumbai on 16th January 2015.

Separation processes are very crucial in nuclear power programme. Use of suitable extractants, chromatographic resins, membranes and precipitants along with process equipment is basis of treatment and management of radioactive waste. Molecular modeling, which encompasses all theoretical methods and computational techniques to model or mimic the behaviour of molecules, is emerging as important tool to design and simulate extractants for solvent extraction processes, stationary phases for chromatographic separation processes, polymeric network for membranes and highly selective precipitants.

I congratulate the organisers for planning this theme meeting which will provide BARC scientists a forum to learn and discuss the application of advanced molecular modeling and simulation methods in separation processes related to nuclear energy programme.

I wish AMMSP-2015 theme meeting a grand success.

Sekhar Basu
(Sekhar Basu)

December 31, 2014

परमाणु ऊर्जा सेवा में परमाणु
BARC
ATOMS IN THE SERVICE OF THE NATION

भाभा परमाणु अनुसंधान केंद्र, ट्रॉम्बे, मुंबई - 400 085, भारत • Bhabha Atomic Research Centre, Trombay, Mumbai 400 085, India
दूरभाष / Phone: +(91) (22) 2550 5300, 2551 1910 • तार: बार्क - मुंबई - 400 085 • Gram: BARC-MUMBAI - 400 085
फैक्स / Fax: +(91) (22) 2559 2107, 2550 5151
ई-मेल / E-mail: basus@barc.gov.in / director@barc.gov.in

पी. के. वातल
P.K. Wattal
निदेशक, नाभिकीय पुन:चक्रण वर्ग
Director, Nuclear Recycle Group

भारत सरकार
Government of India

भाभा परमाणु अनुसंधान केंद्र,
ट्रॉम्बे, मुंबई - 400 085
भारत
Bhabha Atomic Research Centre
Trombay, Mumbai 400 085
India

Message

I am delighted to know that Chemical Engineering Division is organizing one day theme meeting on "Applications of Molecular Modeling in Separation Processes" on January 16, 2015, which prospects to the understanding of classical and advanced computational techniques along with their implication for tackling many important problems in the development and design of chemical engineering systems and separation processes. Today, power of molecular modeling is growing rapidly with the continuing development of computer power, new and robust algorithms, and the availability of software, which would be very supportive to innumerable R&D works. Molecular modeling has resolved many difficulties starting from the defining of structural morphologies to understanding of driving factors associated to various chemical processes especially separation sciences. Understanding of molecular modeling and simulations become very important to provide useful estimates of the parameters and behavior needed to do traditional chemical engineering process development & design.

I wish that theme meeting would provide participants an opportunity to interact with the leading scientists in various fields of separation science and evolve advanced computational approaches to address many challenges in separation science.

I wish the theme meeting a great success.

6.1.15

(P.K. Wattal)

January 6, 2015

दूरभाष / Phone: +(91) (22) 2559 3652 • तार: बार्क - मुंबई - 400 085 • Gram: BARC-MUMBAI - 400 085
फैक्स / Fax: +(91) (22) 2550 5185 • ई-मेल / E-mail: wattal@barc.gov.in

Contents

Molecular Simulation of Diffusion and Selective Complexation in Separation Processes

Meena B. Singh, Jyotsna S. Arora and V. G. Gaikar

Chemical Engineering Department,
Institute of Chemical Technology, Mumbai-400019

Email: vg.gaikar@ictmumbai.edu.in

Abstract. The separation and purification of a single species from mixtures with similar compounds depends on factors such as solution composition, concentration, pH and the nature of cosolutes. Molecular modeling (MM) tools help in understanding the important properties of solutions and in designing new host molecules (ligands) which are extremely selective for the guest molecule. Selectivity is determined by the chemical nature of these molecules and their overall size and shape. The MM methodology has been used for complexation and diffusion of metal ions, purification of natural products, and adsorption of CO_2. Enhanced separation and selectivitycan be successfully achieved with the specific ligands.

Keywords: ligand, natural products, metal ions, CO_2, salvation, molecular simulation

INTRODUCTION

Industrial wastes contain toxic metal ions[1] and greenhouse gases[2] and hence a significant need exists to separate them from both the environmental and industrial process streams. Similarly, the extraction of natural products using organic solvents results in a very complex extract consisting of several unwanted components.[3] To understand these systems, knowledge of solution chemistry can be very helpful. Molecular modeling studies provide perhaps the most powerful tool to elucidate the molecular properties of these designer ligands like the cavity shape, conformations, dimension and available sites for interaction with the desired species and the experimental selectivity with the ligands can be assertively predicted.

COMPUTATIONAL PROTOCOLS

A GROMACS code and Forcite module in Accelrys 4.0 have been used to perform the MD simulations while the Dmol^3 module in Accelrys 4.0 and Gaussian 09 were employed for the Density Functional Theory (DFT) calculations.

Solvation studies of LiCl

Radial distribution function (RDF) and coordination number (CN) of Li^+ ions obtained by the MD simulations are useful for identifying the coordination structures in the solutions and also provide information of time dependent behaviour of each participating species in the system (Diffusion coefficient, D). The D of Li^+ ions decreases with an increase in LiCl concentration which is influenced by the size and type of coordination structure formed in the salt solutions (Fig. 1). The comparison of the density values for LiCl solutions and predicted "D" of all species show a good agreement with experimental values[5].

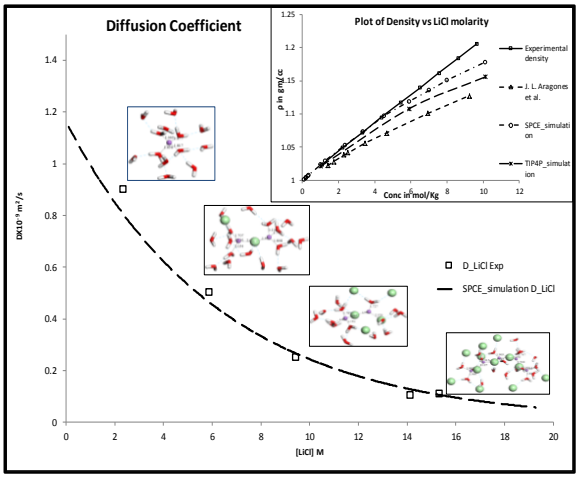

Fig. 1. *Diffusion coefficients of LiCl molecules are plotted as a function of salt concentration and compared with the experimental values[4,5].*

Ligand designing for metal ion separation

A hexa-aza ligand (Fig. 2a) was designed using the DFT for selective adsoprtion of Co(II). The hexa-aza ligand has two fused planar phenanthroline rings and provides a suitable cavity size for Co(II) to fit in. In the optimized

complexes, Co(II) ion sits at the center of the ligand cavity (Fig. 2b). Being larger in size, zirconium cation cannot enter into the ligand cavity and lies above the plane of hexa-aza ligand along with the counterions as shown in Fig. 2c. The selectivity of the ligands toward Co(II) over Zr(IV) was analyzed by comparing interaction energies (IE) of the ligands with the metal ions.[6]

$$IE = E_{complex} - (E_{M^{2+}} + E_L + nE_{Cl^-})$$

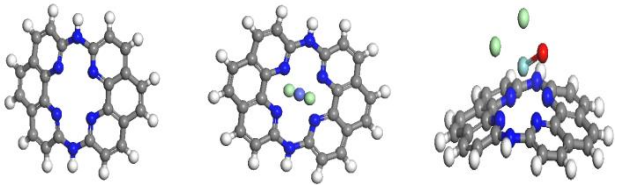

(a) ***Uncomplexed Hexa-aza ligand*** | ***(b)*** ***IE=-79.37 kcal/mol*** | ***(c)*** ***IE=-67.68 kcal/mol***

Fig 2: *DFT-optimized geometry of (a)Hexa-aza ligand with (b) $CoCl_2$ and (c) $ZrOCl_2$ complexes*

Separation of Natural Products

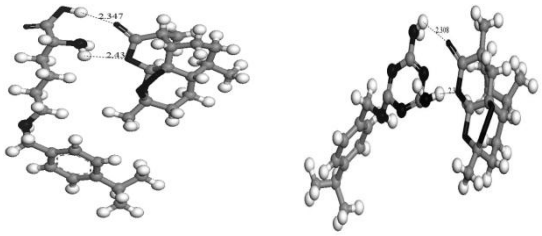

(a) ***IE= -1.5 kcal/mol*** | ***(b)*** ***IE = -32 kcal/mol***

Fig. 3. *DFT derived structure for the interaction of Artemisinin with (a)PS-Lysine and (b)PS-Melamine*

Lysine and melamine loaded polymers were designed as selective adsorbents on the basis of their specific interactions with Artemisinin by DFT calculations (Fig. 3). These studies in gas phase and solvation in MeOH and EtOAc (Table 1) suggest the use of melamine loaded polymer as a selective adsorbent for Artemisinin.[3]

Table 1*: DFT Interaction energy values of ligands*

Component	***DFT, IE, (kcal/mol)***	***MM calculations, IE (kcal/mol)***	
		Solvent	
		MeOH	***EtOAc***
Lysine loaded ligand			
Artemisinin	-1.5	-87	-76
Artemisinic acid	-1.0	-35	-38
Melamine loaded ligand			
Artemisinin	-32	-95	-94
Artemisinic acid	-15	-21	-36

DFT studies for the adsorption of CO_2

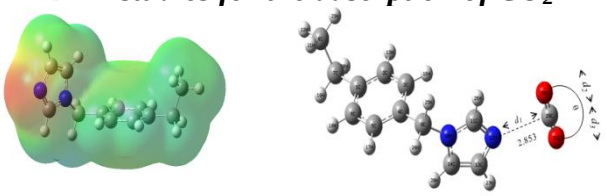

MESP of PS-Imidazole | PS-Imidazole+CO_2

Fig 4: *(a) Calculated mapped electrostatic potential (MEP) surface of PS-Imidazole and (b) DFT-optimized geometry of* PS-Imidazole+CO_2

Table 2: *DFT optimized Interaction Energy (IE), charge Transfer (Q_T) and vibrational frequencies (ν_3) for adsorbent-CO_2 complexes*[2]

Adsorbents	***IE, kcal/ mol***	***d_1*, Å**	**Q_T**	***ν_3^a, cm^{-1}***	***ν_3 cm^{-1}***
CO_2				2333	2349[b]
PS-Imidazole	-11.85	2.8533	-0.009	2326	2335
PS-Piperazine	-6.66	2.9933	-0.012	2324	2336
PS-DMA	-5.08	3.1346	-0.005	2328	2348
PS-DEA	-2.67	2.9013 2.2023 2.7061	-0.011	2333	2348

The electrostatic interactions were responsible for the complexation of CO_2 with the adsorbents. PS-Imidazole shows the strongest interaction with CO_2 (ΔE = -11.85 kJ mol-1) followed by PS-Piperazine > PS-DMA and least for PS-DEA as evident from the interaction energies and distance between CO_2-donor atom of the adsorbent (d_1). H-bonding between –OH groups of DEA and 'O' of CO2 occurs as 'N' atom of DEA is sterically hindered. The calculated vibrational frequency values (ν_3^a) clearly indicate that CO_2 is slightly distorted from its linear shape in the complex and these calculated frequencies exhibit good correlation with experimental values (ν_3)[8] (Table 2).

REFERENCES

1. L. A. S. Santiago, J. A. R. Aguilera, M. P. Gonzalez, D. C.Gonzalez, and M. A.-Rodríguez, *Ind. Eng. Chem. Res.*, 2012, 51, 15184−92.
2. R. S. Madyal and J. S.Arora, *RSC Adv.*, 2014, 4, 20323-33.
3. A. R. Patil, J. S. Arora and V. G. Gaikar, *Sep. Sci. Technol.*, 2012, 47, 1156.
4. F. Stallmach, Department of Physics, University of Leipzig, Personal Communication (2012)
5. M. S. Singh and V G Gaikar, RSC Advances, communicated for publication(2014)
6. P. Kumar, R. S. Madyal, U. Joshi, and V. G. Gaikar, *Ind. Eng. Chem. Res.*, 2011, 50, 8195–03.
7. J. L. Aragones, M. Rovere, C. Vega, and P. Gallo, *J. Phys. Chem. B,* 2014, 118, 7680−91.
8. K. M. Khot, P. K. Heer, R. Biniwale and V. G. Gaikar, *Sep. Sci. Technol.*, 2014, 49 (15), 2376-88.

Theoretical Prediction and Experimental Validation of New Actinide Selective Ligands

Tapan K. Ghanty
Theoretical Chemistry Section, Chemistry Group
Bhabha Atomic Research Centre, Mumbai-400085

Email: tapang@barc.gov.in

Abstract. The conventional concept of selective complexation of actinides with soft donor ligands (either S or N donor) has been modified here through exploiting the concept, "intra-ligand synergism", where hard donor atom, such as, oxygen preferentially binds to trivalent actinides [An(III)] as compared to the valence iso-electronic trivalent lanthanides [Ln(III)] in presence of another soft donor centre. We have theoretically predicted the selectivity of 1,10-phenanthroline-2,9- dicarboxylamide (PDAM) towards Am(III) ion through density functional calculations. Subsequently, several such amide derivatives have been synthesized to optimize the solubility of the ligands in organic phase. Finally, solvent extraction experiments have been carried out to validate our theoretical prediction on the selectivity of oxygen donor ligands towards Am(III) as compared to Eu(III), and a maximum separation factor of about 51 has been achieved experimentally using 2,9-bis(N-decylaminocarbonyl)-1,10-phenanthroline ligand.

Keywords: Density functional theory, Americium, Europium, 1,10-phenanthroline-2,9-dicarboxylamide, Separation factor

INTRODUCTION

In recent years, considerable attention has been given to understand the coordination chemistry of trivalent lanthanide (Ln) and actinide (An) with various ligands because of its close link with the nuclear waste management steps. This is a challenging and difficult task because of very similar chemical properties of these two series of ions as they have similar ionic radii and coordination numbers. The hard soft acid base principle (HSAB)[1] classifies the Ln(III) and An(III) cations as hard Lewis acids, consequently their bonding is primarily ionic and mainly governed by charge density. Despite this, there is a modest enhancement of covalency in the bonding of An(III) with various ligands as compared to that in Ln(III) complexes due to the larger spatial extent of the 5f shell of actinides as compared to the 4f shell in lanthanides. Because of this, an advantageous discrimination between An(III) and Ln(III) ions is possible while using ligands with soft donor atoms like sulfur and nitrogen.[2] It is important to note that efficiency of complex formation of either Ln(III) or An(III) with oxygen donors is much better as compared to N or S donors because both the set of metal ions are hard Lewis acids, however no selectivity is observed with O donor ligands. We have proposed a new concept, "intra-ligand synergism",[3] and exploited[4] it for the selective complexation of actinides with O donor in presence of N donor available in the same ligand.

COMPUTATIONAL METHODOLOGY

All the geometries of the bare ligands and the metal-ligand complexes have been optimized using DFT with BP86 exchange-correlation functional without any symmetry restrictions. We have used two different program packages, viz., Turbomole 6.3[5] and ADF2010.01 to carry out the theoretical calculations.[6] In Turbomole, 28 and 60 electron core pseudo potentials (ECP) along with the corresponding def-SV(P) basis sets have been used for the lanthanide (Eu) and Actinide (Am) ions, respectively. For the lighter atoms, all electron def-SV(P) basis sets have been used. Solvent effect has been considered using COSMO approach with dodecane as solvent (epsilon=2). For ADF calculations Slater type orbital (STO) basis set added with two polarization functions (TZ2P) along with frozen core approximations have been used. The frozen cores considered for various atoms are 1*s*-4*d* for lanthanides, 1*s*-5*d* for actinides, and 1*s* for carbon, nitrogen and oxygen. Bond critical point (BCP) properties (electron density [ρ], Laplacian of the electron density [$\nabla^2\rho$]) have also been calculated within the framework of quantum theory of atoms-in-molecule (AIM) approach.[7]

RESULTS AND DISCUSSIONS

Here we have considered three different stoichometries for the complexes, viz., $[M(PDAM)_2]^{3+}$, $[M(PDAM)_2NO_3]^{2+}$ and $[M(PDAM)(NO3)_3]$. The optimized geometrical parameters in the gas phase and the complexation energies in both gas and solvent phases are reported in TABLE 1. From the calculated metal-ligand bond distances (M-O and M-N) it is clear that the Am-N and Am-O bond lengths are slightly shorter as compared to the corresponding Eu-N and Eu-O bond lengths. It is also interesting to note that there are considerable differences in bond length values between the Am^{3+} and Eu^{3+} complexes for the $[M(PDAM)_2NO_3]^{2+}$

and [M(PDAM)$(NO_3)_3$] compositions.

TABLE 1. Calculated M-L bond distances (Å) and complexation energies (eV) in gas (ΔE_g) and solvent (ΔE_s) phases for Am^{3+} and Eu^{3+} complexes

Complexes	M-N	M-O/M-S	ΔE_g	ΔE_s
[Am-(PDAM)$_2$]$^{3+}$	2.605	2.408	-29.64	-2.33
[Eu-(PDAM)$_2$]$^{3+}$	2.612	2.402	-30.33	0.86
[Am-(PDAM-Isobutyl)$_2$]$^{3+}$	2.604	2.371	-28.97	-1.16
[Eu-(PDAM-Isobutyl)$_2$]$^{3+}$	2.603	2.363	-29.91	1.77
[Am-(PDAM-Decyl)$_2$]$^{3+}$	2.615	2.409	-30.32	-2.30
[Eu-(PDAM-Decyl)$_2$]$^{3+}$	2.681	2.449	-31.46	0.78
[Am-(PDAM)$_2$(NO_3)]$^{2+}$	2.648	2.527	-38.98	-8.92
[Eu-(PDAM)$_2$(NO_3)]$^{2+}$	2.677	2.520	-39.72	-5.65
[Am-(PDAM)(NO_3)$_3$]	2.657	2.496	-48.38	-6.53
[Eu-(PDAM)(NO_3)$_3$]	2.713	2.537	-48.96	-2.93

TABLE 2 Percentage electrostatic, Pauli, steric and orbital interactions in the total bonding energy as obtained from energy decomposition analysis

Complex Name	% electrostatic interaction	% Pauli interaction	% steric interaction	% orbital interaction
[Am-DAM]$^{3+}$	77.40	-40.53	36.87	63.12
[Eu-PDAM]$^{3+}$	70.05	-31.00	39.05	63.95

TABLE 3. Calculated BCP properties (electron density [ρ], Laplacian of the electron density [$\nabla^2\rho$]) of the M-N and M-O/M-S bonds in Am^{3+} and Eu^{3+} complexes

Bond	M-N		M-O/M-S	
	ρ (e a_0^{-3})	$(-1/4)\nabla^2\rho$ (e a_0^{-5})	ρ (e a_0^{-3})	$(-1/4)\nabla^2\rho$ (e a_0^{-5})
[Am-PDAM]$^{3+}$	0.0315	-0.0239	0.0461	-0.0410
[Eu-PDAM]$^{3+}$	0.0237	-0.0184	0.0340	-0.0337

TABLE 4. Calculated atomic charges on metal and donor centers of Am^{3+} and Eu^{3+} complexes

Complexes	q_M	$q_{O/S}$	q_N
[Am-(PDAM)$_2$]$^{3+}$	1.734	-0.659	-0.522
[Eu-(PDAM)$_2$]$^{3+}$	1.659	-0.649	-0.507

A higher percentage of orbital interaction component (TABLE 2) and higher values of BCP ρ and $\nabla^2\rho$ (TABLE 3) imply that the Am^{3+} complexes with amide based ligands are more covalent in nature as compared to the corresponding Eu^{3+} complexes. At the same time, higher charge on the Am centre (Table 4) indicates that the Am^{3+} complexes with amide based ligands are slightly more ionic in character as compared to the corresponding Eu^{3+} complexes. Thus, it is expected that the combined effects of higher orbital mixing, which provides additional covalency to the Am-L bonds and the larger ionic interaction provided by the hard donor oxygen in the mixed donor ligands make the amide ligands selective towards Am^{3+} over Eu^{3+}.

Due to the solubility problem of the PDAM ligand in organic diluents, we have alkylated the amide groups of PDAM through which its solubility in organic medium has been enhanced. Therefore, three amide ligands viz, PDAM, PDAM-Isobutyl and PDAM-Decyl have been synthesized. Subsequently, the extraction efficiency of these ligands have been investigated using solvent extraction technique and it has been found that all the alkyl derivatives of PDAM ligand are Am^{3+} selective. A maximum extraction efficiency and separation of Am^{3+} over Eu^{3+} has been observed experimentally using the ligand PDAM-Decyl as compared to the other ligands reported here (Figures 1 and 2).[4]

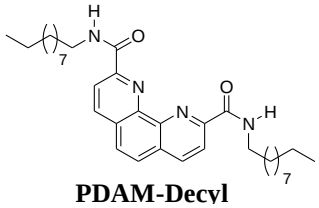

PDAM-Decyl

FIGURE.1 Schematic depiction of structures of PDAM-Decyl.

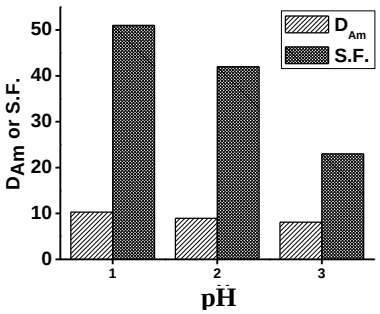

FIGURE.2 Effect of pH on the Distribution and separation behavior of Am^{3+} and Eu^{3+} using PDAM-Decyl. Org. Phase: 8 x 10^{-3} M PDAM-Decyl in dodecane:octanol (5:1) mixture
Aq. Phase: 2M $LiClO_4$ at different pH

TABLE 5. Distribution and separation behaviour of Am^{3+} and Eu^{3+} using the amide ligands

Ligand	D_{Am}	D_{Eu}	S.F.
PDAM	21.4	2.9	7.4
PDAM-Isobutyl	4.62	1.05	4.4
PDAM-Decyl	10.3	0.2	51

ACKNOWLEDGEMENTS

It is a pleasure to thank my coworkers, Ms. Debashree Manna, Dr. S. Mula, Dr. A. Bhattacharyya and Dr. S. Chattopadhyay. Computer Division, BARC is gratefully acknowledged for providing parallel computational facility.

REFERENCES

1. R. G. Parr and R. G. Pearson, *J. Am. Chem. Soc.* **105**, 7512-7516 (1983).
2. R. M. Diamond, K. Street and G. T. Seaborg, *J. Am. Chem. Soc.* **76**, 1461-1469 (1954).
3. D. Manna and T. K. Ghanty *Phys. Chem. Chem. Phys.*, **14**, 11060-11069 (2012).
4. D. Manna, S. Mula, A. Bhattacharyya, S. Chattopadhyay and T. K. Ghanty, Dalton Trans. **44**, 1332-1340 (2015).
5. TURBOMOLE is program package developed by the Quantum Chemistry Group at the University of Karlsruhe, Germany, 1988**:** R. Ahlrichs, M. Bär, M. Häser, H. Horn and C. Kölmel, *Chem. Phys. Lett*. **162**, 165-169 (1989).
6. ADF2010.01, SCM, Theoretical Chemistry, Vrije Universiteit, Amsterdam, The Netherlands; http://www.scm.com.
7. R. F.W. Bader, *Atoms in Molecules-A Quantum Theory* (Oxford University Press, Oxford, 1990).

Molecular Modeling Guided Experiments for Separation of Isotope and Metal Ions

Sk. Musharaf Ali, A. Boda, A.K. Singha Deb, P. Sahu, K.T. Shenoy
Chemical Engineering Division,
Bhabha Atomic Research Centre, Mumbai-400085
Homi Bhabha National Institute

Email: musharaf@barc.gov.in

Abstract. DFT based electronic structure calculations were performed to evaluate the isotope separation factor of Gd with cyclic polyethers and functionalized polyethers. The reduced partition function ratio (RPFR) and isotope separation factor (α) for hydrated Gd^{3+} ion and complexes with ligands are computed using standard method. The calculated separation factor was found to be in good agreement with the experimental data. Theoretical investigation of the extraction of Eu(III) and Am(III) with diglycolamic acid functionalized carbon nanotubes (CNT-DGA) has also been carried out using DFT. The calculated free energy of extraction, ΔG_{ext} is found to be higher with Eu^{3+} over Am^{3+} and same is confirmed from the experimental results.

Keywords: Gadolinium isotope, DB18C6, DFT, Separation factor, Free energy, Eu^{3+}, Am^{3+}, CNT-DGA**.**

INTRODUCTION

Molecular modeling that comprises Quantum mechanics (QM), Monte-Carlo (MC) molecular dynamics (MD) and ab initio MD (AIMD) simulation has been emerged as a prospective tool for the calculation of various molecular properties by capturing the complex molecular interactions and is practiced in the widespread fields of science and engineering [1]. In that context, design and screening of suitable ligands for efficient separation of metal ions is very imperative and demanding in view of the safe removal of nuclear and chemical waste employing the much practiced separation methodologies namely: solvent extraction and chromatographic separation. In solvent extraction, metal ions from the aqueous solutions are extracted by ligands/extractants of the organic phase and in chromatographic separation, functional group/ligand fixed on a solid matrix captures selectively the metal ions of interest which would be eluted in the next step. Use of suitable ligand/extractants is necessary for establishing efficient separation processes.

Macrocyclic crown ether ligands have been tested for isotope separation in addition to its strong affinity for metal ion complexation [2]. Natural Gadolinium is currently used as a burnable poison in nuclear fuel. Use of Gd-155 and 157 would create an even more effective burnable poison. Gd-157 (254,000 barn) and Gd-155 (60,900 barn) has the highest cross section for the capture of thermal neutrons. All the remaining isotopes are having lower values Gd-152(735 barn), Gd-154 (85 barn), Gd-156 (18 barn), Gd-158 (2.2 barn), Gd-160(1.4 barn). Use of Gd-155/157 would create more effective burnable poison. It will be worthwhile to investigate whether cyclic crown ether can also be used for isotope separation of Gadolinium.

Due to their large specific surface area and small size, highly porous, hollow structures, low mass density, high mechanical, thermal and chemical stabilities, carbon nanotubes (CNTs) have drawn great attention as a promising adsorbent for the separation of various inorganic, organic and radioactive pollutants [3]. The adsorption capacity, efficiency and selectivity of CNTs can be tailored by modifying its surface with organic complexing functionalities. Diglycolamic acid (DGA) derivatives, a CHON type anionic tridentate ligand, are emerging as potential candidate for trivalent lanthanide-actinide separation [4]. DGA modified CNTs may be a viable sorbents for this separation.

THEORY

The gadolinium isotopic exchange for heavy (H) and lighter isotope (L) between two phases is written as

$$^{H}Gd^{3+}_{(aq)} + {}^{L}Gd^{3+}_{(comp)} \rightarrow {}^{L}Gd^{3+}_{(aq)} + {}^{H}Gd^{3+}_{(compl)}. \quad (1)$$

The separation factor, α for the above exchange reaction

$$\alpha = f^{r}_{Gd^{3+}(aq)} / f^{r}_{Gd^{3+}(compl)} \quad (2)$$

can be written in terms of reduced partition function ratio (RPFR, f^{r}) [5] as follows:

$$f^{r} = \frac{Z_{vib,{}^{H}Gd^{3+}} \prod \frac{h\nu_{i,{}^{H}Gd^{3+}}}{k_b T}}{Z_{vib,{}^{L}Gd^{3+}} \prod \frac{h\nu_{i,{}^{L}Gd^{3+}}}{k_b T}} \quad (3)$$

Here, $Z_{vib,^{H}Gd^{3+}}$ is the vibrational partition function of molecular species with $^{H}Gd^{3+}$ isotope and ν_i is the harmonic frequency. The k_B, h and T are the Boltzmann Planck constant and temperature, respectively. The main input required for the evaluation of RPFR is the harmonic vibrational frequency, which can be obtained either experimentally or computationally.

COMPUTATIONAL PROTOCOL

All the geometries of the free as well complexes are optimized using Turbomole [6] package at BP86/SVP level of theory [7]. Single point energy calculations were carried out on optimized complexes at B3LYP/TZVP [8, 9] level of theory. The optimized structures of various ligands and their metal ion complexes are drawn using MOLDEN molecular visualization graphics programme.

Effective core potential (ECP) for both Eu and Am was used where 28 electrons were kept in the core for Eu and 60 for Am [10]. The spin of both Eu^{3+} and Am^{3+} ions was taken as septet state. The zero point energy and thermodynamic correction to the total energy were made to compute the free energy at T=298.15K. The geometries were optimized with BP86 functional but total energies were calculated using B3LYP functional. The solvent effect in the energetic was incorporated employing conductor line screening model (COSMO) [11]. One of the key properties to be calculated in the metal ion-ligand complexation is the free energy of extraction (ΔG_{ext}). The metal ion-ligand complexation reaction is modelled using the following reaction as follows:

$$M^{3+}_{(aq)} + 3NO_3^-{}_{(aq)} + CNT\text{-}DGA_{(aq)} \xrightarrow{\Delta G_{ext}} [CNT\text{-}DGA\text{-}M(NO_3)_3]_{(aq)}, \quad (M=Eu/Am) \qquad (4)$$

The change in Gibbs free energy of extraction, ΔG_{ext}, in Equation 4 can be obtained by the thermodynamic cycle [12] (Born-Haber) (Fig. 1) in terms of the free energy change in gas phase, $\Delta G_{(gp)}$, and the solvation free energies of the products and reactants, $\Delta\Delta G_{(sol)}$. The overall complexation reaction is characterized by the free energy of extraction, ΔG_{ext} as

$$\Delta G_{ext} = \Delta G_{(gp)} + \Delta\Delta G_{(sol)} \qquad (5)$$

Where, $\Delta G_{(gp)}$ is expressed as

$$\Delta G_{(gp)} = \Delta E_{(gp)} + \Delta ZPE + \Delta nRT - T\Delta S \qquad (6)$$

Here, $\Delta E_{(gp)}$, ΔZPE, Δn, and ΔS are the change in total electronic energy, change in zero point energy, change in number of molecules and change in entropy for the reaction, respectively. R is the Universal gas constant. The solvation free energies of the products and reactants, $\Delta\Delta G_{(sol)}$, is computed as:

$$\Delta\Delta G_{(sol)} = \Delta G_{CNT-DGA-M(NO_3)_3(sol)} - (\Delta G_{M^{3+}(sol)} + 3\Delta G_{NO_3^-(sol)} + \Delta G_{CNT-DGA(sol)}) \qquad (7)$$

Where, $\Delta G_{(sol)}$ is the solvation free energy of the respective species.

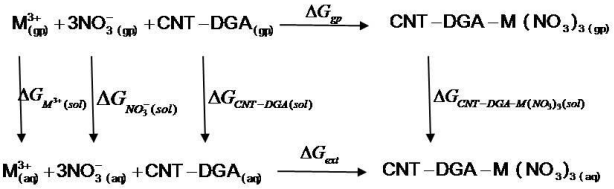

Fig. 1. Thermodynamic cycle for calculation of free energy of extraction for Eu^{3+} and Am^{3+} ion with CNT-DGA.

RESULTS AND DISCUSSIONS

Most of the isotopic enrichment of the elements takes place from aqueous feed solution. Therefore, it is of primary importance to understand the solvation/hydration sphere structure of the metal ion of interest. For any quantum computation, the structure of the system under study has to be considered first. Hence, we have optimized the nonahydrated structure of gadolinium metal ion ($Gd^{3+}(H_2O)_9$) and is displayed in Fig. 1. The nonahydrated structure has been reported earlier using EXAFS[13]. The calculated Gd-O distance (2.52Å) is well matched with the EXAFS data (2.39Å) [13]. The corresponding IR frequency is presented in Fig. 2. Three crown ethers namely DCH18C6, B15C5 and DB18C6 were used in the complexation studies of Gd^{3+} ion.

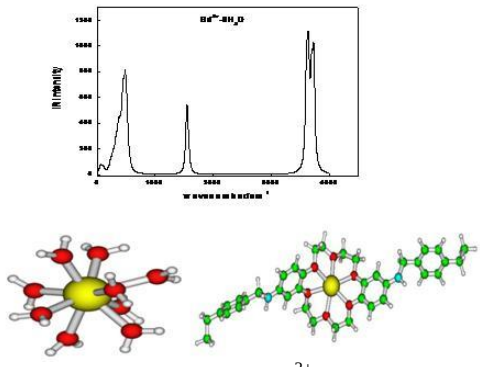

Fig. 2. Optimized complex of Gd^{3+} ion with water and CMPS-DB18C6 and IR frequency of hydrated Gd^{3+} ion.

The RPFR of Gd (155/160) is found to be more than Gd (157/160) in all the studied complexes as shown in Table. 1. The reduced partition function ratio (RPFR) and isotope separation factor (α) for hydrated Gd^{3+} ion and complexes of Gd^{3+} with B15C5, DB18C6 and DCH18C6 are computed. In the case of DOWEX resin, observed separation factors are 1.000102 and 1.000086

for isotopic pairs of Gd (155/160) and Gd (157/160) respectively which are close to the reported experimental values of 1.000064 and 1.000040 respectively [14]. The separation factor for Gd (155/160) is more compared to Gd (157/160) due to larger mass difference (Δm) in the case of Gd (155/160). The results show that the separation factor with DB18C6 is higher when compared to B15C5, DCH18C6. In view of its comparatively higher separation factor DB18C6 is considered to be promising ligand for isotopic enrichment of gadolinium. But, in order to get considerable amount of enriched isotopes, the crown ether ligand should be grafted on some solid matrix and then the isotopic separation can be carried out in columnar mode. To meet these criteria, DB18C6 is grafted on chloromethylated polystyrene (CMPS) resin. In order to keep the molecular system computationally tractable, only one DB18C6 was anchored on one molecular unit of CMPS resin. The optimized structures of Gd^{3+} complexes with CMPS-DB18C6 are displayed in Fig. 2 and the computed α values are shown in Table 1. The predictability of the computational protocol was validated by using the reported results of commercially available DOWEX resin with EDTA as complexing/enrichment agent. Furthermore, the calculated separation factor for 152/160 pair for Gd^{3+}-DCH18C6 (α=1.0012) was found to be in good agreement with the reported experimental results (α=1.002) [15] and thus confirms the acceptability of the present methods of modeling the isotope separation [16]. This will be discussed in details in the talk.

Table 1. Calculated values of RPFR and separation factor values of Gd in different complexes.

Complex of Gd^{3+}	RPFR(f^r)		$\alpha_{155/160}$	$\alpha_{157/160}$
	$Gd_{155/160}$	$Gd_{157/160}$		
9w	1.0024	1.0014		
EDTA	1.00151	1.000914	1.000102 (1.000064)	1.000086 (1.000040)
DCH18C6	1.001890	1.001083	1.000509	1.000317
DB18C6	1.000647	1.000391	1.001752	1.001009
B15C5	1.002016	1.001213	1.000383	1.000187
CMPS-DB18C6	1.001191	1.000712	1.0012	1.00068

We have considered one DGA unit anchored on the open pore of the (8,0) zig-zag CNT with 4 unit cells as earlier studied for one unit of carboxylate anchored on CNT [17]. The optimized geometries of CNT-DGA and their complexes with trivalent Eu^{3+} and Am^{3+} ions in absence of nitrate ions and the calculated structural parameters are displayed in Fig. 3 and Table 2, respectively.

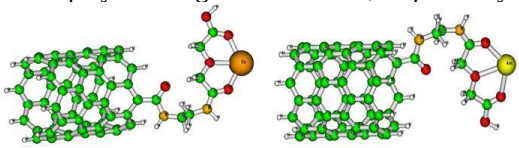

Fig.3. Optimized structures of Eu and Am with DGA-CNTs

Both the Eu^{3+} and Am^{3+} ions are found to be directly coordinated to the three donor O atoms of the DGA moiety. All three donor O atoms and the coordinated metal ion are lying in the same plane. It is interesting to mention that though the metal ions and three donor O atoms are lying in the same plane, the M-O bond length with three O atoms are not same in length. The M-O (O of C=O group) bond length was found to be 2.292 and 2.391Å and one M-O (ethereal O) bond length was found to be 2.520Å for Eu^{3+} ion, whereas for Am^{3+} ion it was 2.324, 2.419 and 2.596Å respectively. The shorter M-O bond length for C=O group compared to M-O bond length of ethereal O suggest that former has stronger interaction ability than the later. The shorter bond length of Eu^{3+} compared to Am^{3+} ion in absence of nitrate ion might be due to the higher covalency in Eu-O bond compared to Am-O bond. The larger C=O distances and smaller M-O distances for Eu^{3+} compared to Am^{3+} points towards strong interaction of the former with the CNT-DGA than the later. The optimized structure of Eu^{3+} and Am^{3+} ion in presence of nitrate ion is displayed in Fig. 4. Both the Eu^{3+} and Am^{3+} ions are found to be nona coordinated through 3 donor atoms from DGA and six donor atoms from three nitrate ions in bidentate mode. The Eu-O (oxygen of NO_3) is found to be varied from 2.449 to 2.534Å whereas Am-O (oxygen of NO_3) is found to be varied from 2.425 to 2.515Å. The Eu-O (carbonyl oxygen of DGA) is found to be varied from 2.566 to 2.694Å and for Am-O (carbonyl oxygen of DGA) is found to be in the range of 2.457 to 2.665Å indicating asymmetrical nature of bonding from the identical carbonyl bonding. The Eu-O (etheric oxygen of DGA) is found to be 2.611Å and for Am^{3+} it is determined to be 2.618Å. The close M-O bond distance bears the fact that trivalent lanthanides and actinides have similar chemical properties. The calculated Eu-O bond distances of hydrated metal ions were found to be varied from 2.454-2.539Å, whereas, the same Am-O bond distance were found to be varied form 2.508-2.589Å suggesting that the hydration energy of Eu^{3+} ion should be more than that of Am^{3+} ion due to shorter bond length of Eu-O over Am-O. Further, the M-O bond length in hydrated species was found to be larger than the M-O bond length of C=O group of DGA ligand. The M-O bond distance of NO_3^- ion is found to be smaller than the M-O of H_2O indicating the stronger interaction of metal ions with NO_3^- ion group than H_2O.

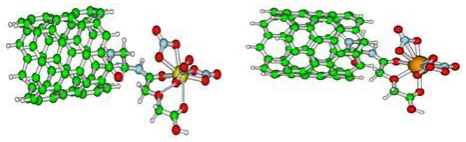

Fig. 4. Optimized structures of nitrate complexes of Am and Eu with DGA-CNTs.

Table 2. Calculated structural parameters of complexes of Eu^{3+} and $Am3^{+}$ with CNT-DGA at BP86/SVP level of theory.

d_{M3+-O} (Å)of	with Nitrate		without Nitrate	
	Am^{3+}	Eu^{3+}	Am^{3+}	Eu^{3+}
NO_3(1)	2.448	2.459	-	-
	2.425	2.449		
NO_3(2)	2.456	2.475	-	-
	2.463	2.534		
NO_3(3)	2.457	2.475	-	-
	2.515	2.483		
DGA-C=O	2.457	2.566	2.419	2.391
	2.665	2.694	2.324	2.292
DGA-C-O-C	2.618	2.611	2.596	2.520

Table 3. Calculated value of thermodynamic parameters (kcal/mol) for the extraction of Eu^{3+} and Am^{3+} ions with CNT-DGA at B3LYP/TZVP level of theory

M^{3+}	ΔG_{gp}	$\Delta G_{(sol)}$ (M)	$\Delta G_{(sol)}$ (CNT-DGA)	$\Delta G_{(sol)}$ (CNT-DGA-M(NO3)3)	ΔG_{ext}
Eu	-1015.0	-820.2	-34.6	-46.8	-44.3
Am	-993.2	-799.4	-34.6	-43.8	-40.3

From Eq. 5, it is seen that the free energy of extraction, ΔG_{ext} has two contributory components, one is assigned from the gas phase and other one is from the solvent phase. The calculated values of $\Delta\Delta G_{sol}$ is presented in Table 3. From the Table, it is seen that in presence of nitrate ion, the value of $\Delta G_{(gp)}$ supersedes the positive value of $\Delta\Delta G_{(sol)}$ for both Eu^{3+} and Am^{3+} leading to negative value of ΔG_{ext} (Table 3). The free energy of Eu^{3+} ion was found to be higher than that of Am^{3+} ion by 3.98kcal/mol. Experimental adsorption of Eu^{3+} and Am^{3+} from aqueous solution by synthesized DGA-functionalized-MWCNTs have also showed that CNT-DGA have higher sorption capacity values for Eu^{3+} than that of Am^{3+} ions. It is interesting to note that using the simple complexation reaction in solution phase where all the energy calculations are done using implicit solvation leads to higher selectivity for Am^{3+} ion over Eu^{3+} ion in the presence of nitrate ion, whereas using more reliable thermodynamic cycle the selectivity order becomes reversed i.e. Eu^{3+} ion is extracted preferentially over Am^{3+} ion. The suitability of the methodology can be validated by performing the adsorption experiments and same will be discussed in details in the talk.

ACKNOWLEDGEMENTS

Computer Division, BARC is gratefully acknowledged for providing the Anupam parallel computational facility.

REFERENCES

1. A. Chakraborty, Molecular Modeling and Chemical Engineering, Academic Press, 2001, San Diego.
2. Heumann, K. G., Organic Chemistry, Springer 1985, pp. 77-132.
3. (a) X. Ren, C. Chena, M. Nagatsu and X. Wang, *Chem Engg. J*., 170 (2011) 395; (b) A.K. Singha Deb, P. Ilaiyaraja, D. Ponraju, B. Venkatraman, J. *Radioanal. Nucl. Chem*., 291 (2012) 877–883.
4. A.S. Suneesh, K..A. Venkatesan, K.V. Syamala, M.P. Antony, P.R. Vasudeva Rao, *Radiochim. Acta*, 100 (2012) 427.
5. J. Bigeleisen and M.G. Mayer, *J. Chem. Phys*. 15 (1947) 261-267.
6. TurbomoleV6.3, University of Karlsruhe, Germany, 1988.
7. Becke, A. D., *Phys. Rev. A*, 38 (1988) 3098.
8. Becke, A. D., *J. Chem. Phys.*, 98(1993) 1372-1377.
9. Lee, C., Yang, W., Parr, R. G., *Phys. Rev. B* 37 (1988) 785.
10. Dolg, M.; Stoll, H.; Preuss, H. *J. Chem. Phys*. 90 (1989) 1730-1734; Kuchle, W.; Dolg, M.; Stoll, H.; Preuss, H. *J. Chem. Phys*. 100 (1994) 7535-7542; Cao, X; Dolg, M. J. Mol. Structure (THEOCHEM), 673 (2004) 203-209; Cao, X.; Dolg, M.. *J. Mol. Structure (THEOCHEM)*, 581 (2002) 139-147.
11. Klamt, A. *J. Phys. Chem*. 99 (1995) 2224-2235.
12. Sk. M. Ali, *Eur. J. Inorg. Chem*. 9 (2014) 1533; Sk. M.Ali, J.M.Joshi, A.Singha Deb, Anil Boda, K.T.Shenoy and S.K.Ghosh, *RSC Adv*., 4 (2014) 22911-22925; A. Boda and Sk. M.Ali, *J. Phys. Chem. A* 2012, 116, 8615−8623.
13. I. Persson, P. D'Angelo, S De Panfilis, M. Sandstrom and L. Eriksson, *Chem. Eur. J*. 14 (2008) 3056–3066.
14. Ismail, I. M., Fukami, A., Nomura, M., Fujii, Y., *Analytical Chemistry* 72 (2000) 2841-2845.
15. T. Fujii, T. Yamoto, J. Inagawa, K. Gunji, K. Watanabe and K. Nishizawa, *Sol. Ext. Ion. Exch*. 17 (1999) 1219-1229.
16. A.K. Singha Deb, Sk. M. Ali, K.T. Shenoy and S.K. Ghosh, *J. Chem. Eng. Data*, 59 (2014) 2472-2484.
17. A.K. Singha Deb, A. Bhattacharyya, Sk. M. Ali, K.T. Shenoy, S.K. Ghosh, *Mol. Sim*, 2014 (in press); A.K. Singha Deb, A. Bhattacharyya, Sk. M. Ali, K.T. Shenoy, S.K. Ghosh, *Sep. Sci. Tech*., 2014 (in press)

Molecular Simulations In A Computational Scheme For Rational Solvent Design: Extraction Of R-PAC

Madakashira Harini,[1] Jhumpa Adhikari[1], Santosh B. Noronha,[1] and K. Yamuna Rani[2]
[1]*Department of Chemical Engineering, Indian Institute of Technology Bombay, Mumbai-400076, India.*
[2]*Chemical Engineering Division, Indian Institute of Chemical Technology, Hyderabad-500607, India.*

Email: adhikari@che.iitb.ac.in

INTRODUCTION

R-phenylacetylcarbinol (R-PAC) is an intermediate in the manufacture of pharmaceuticals such as pseudoephedrine and ephedrine which find extensive use in cold and influenza medication. Industrially, R-PAC is produced by a whole cell bio-catalysis process with benzaldehyde as the substrate [1]. The product (R-PAC) which is formed in the aqueous phase, is extracted to the organic phase. Current industrial practice employs toluene as the solvent, but efficiency of extraction of the product in toluene is often low and hence, there is need to design a solvent with better extraction properties. To design a solvent with extraction properties which are superior to toluene, we have developed a computational scheme based on the computer aided molecular design (CAMD) algorithm where we have employed the molecular simulation approach to estimate the thermodynamic properties of R-PAC (limited to the vapour pressures at three temperatures including the normal boiling point in literature) required for process design and also, to verify the results obtained from CAMD using molecular simulations.

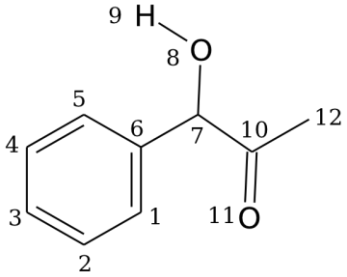

Scheme 1. Structure of PAC. 1-5 CH(aro), 6 C(aro), 7 CH , 8 O(hydroxyl), 9 H(hydroxyl), 10 C(carbonyl), 11 O(Carbonyl), 12 CH_3

COMPUTATIONAL METHOD

The knowledge of thermodynamic properties of R-PAC is essential to improve the process involving the separation of R-PAC from the organic solvent, used in the biotransformation to extract R-PAC from the aqueous broth. In spite of its importance, limited experimental vapour pressure data is available on R-PAC in literature. Hence, the physical and thermodynamic properties of R-PAC are predicted using structure property correlations combined with equations of state (EoS), and also molecular simulations as the first step to optimize the process design for the production of R-PAC. To achieve a better separation of R-PAC, it is essential to have knowledge of certain thermodynamic properties such as normal boiling point (T_b), vapour pressure, density (ρ), critical temperature (T_C), critical pressure (P_C), heat of vaporization (ΔH_{vap}), etc. Experimental vapour-liquid equilibria (VLE) data of R-PAC reported in literature [2] are limited to vapour pressures at three different temperatures, including the T_b. In general, experimental data on property determination exists primarily for low molecular weight compounds or for larger molecules at low temperature; as at higher temperatures many compounds undergo thermal decomposition. Additionally, performing experiments to determine vapour liquid coexistence properties is expensive and time consuming because of the high pressures and temperatures involved. As an alternative, the properties that are of interest to a molecule can be found through quantitative structure property relationships [3] combined with EoS [4]; and also using the Gibbs ensemble Monte Carlo (GEMC) simulation technique [5]. This GEMC technique is combined with transferrable potentials for phase equilibria – united atom (TraPPE-UA) force field where parameters for the torsions not reported in literature are determined using the density functional theory (DFT).

After determination of the properties of R-PAC, we have used CAMD to find organic solvents with extraction properties superior to toluene. As numerous solvents exist, performing experiments to find solvents suitable for specific applications require substantial amount of time and also, experiments may be expensive. The CAMD framework [6] is a reverse engineering approach that can shortlist candidate molecules with specific target properties, by employing structure property correlations and, generally, an optimization technique. Although, the correctness of the estimates of CAMD are solely based on the accuracy of the property estimation method (such as group contribution (GC),

which is "inherently approximate"), the derived molecules from CAMD can be the starting point to further experimentation. Since, solvents may also be expensive, the trends predicted by CAMD can also be verified using the molecular simulation approach whereby the solubility parameter of each of solvents can be determined and compared with the value for R-PAC; with solvents for which the values are close to that of R-PAC being the better solvent.

RESULTS & DISCUSSION

The modelling of VLE is an important source of uncertainties in chemical industry for the design of various separation processes such as distillation, stripping and solvent extraction. The thermodynamic properties of R-PAC, determined using structure property correlations and GEMC simulations, in the absence of extensive experimental data have been determined. In structure property correlations, Marrero-Gani (MG) method [7] reported parameters have been utilized to determine the critical properties and the boiling point of R-PAC. Further, VLE has been determined by the use of various EoS by making use of the predicted critical property data. Alternatively, GEMC-NVT simulations have been carried out to determine VLE and the critical point, where unknown torsions of the PAC molecule (modelled using TraPPE-UA force field) have been determined from the DFT approach. There is an excellent agreement in the coexistence vapour densities from molecular simulation, Peng-Robinson (PR) and volume translated Peng-Robinson (VTPR) EoS. The estimated coexistence liquid densities from molecular simulation match well with the predictions of VTPR EoS using the MG parameters. However, the coexistence liquid densities as predicted by the MG parameters in the VTPR EoS show larger deviation from GEMC results at low temperatures. The normal boiling point temperature determined from GEMC is found to lie in between the predictions of the MG method and the experimentally reported data. The vapour pressures as predicted by GEMC simulations are comparable to the experimental data with increase in temperature.

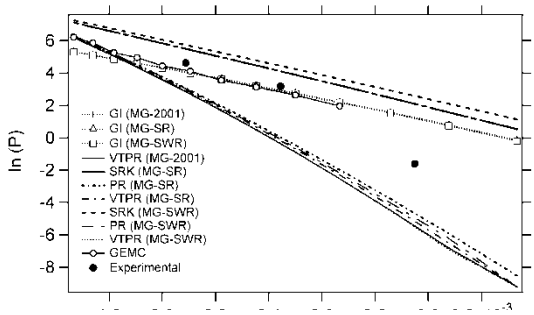

Fig. 1: Comparison between vapor pressures from GI correlation, EoS and GEMC simulations obtained in this work with experimental data

Then, we have employed CAMD as a cost effective tool to design a solvent to extract, R-PAC, efficiently from an aqueous phase. The acyclic aliphatic solvents recommended as superior to toluene from the CAMD method include amyl acetate, methyl pentanone, ethyl pentene and methyl methoxy benzene. Preliminary molecular simulation studies to calculate the solubility parameters indicate that all the above solvents (with the exception of amyl acetate) are superior to toluene. Experiments are on-going to confirm the results.

REFERENCES

1. B. Rosche, V. Sandford, M. Breuer, B. Hauer and P.L. Rogers, *J. Mol. Cat. B: Enzymatic*. 19-20 (2002) 109–115.
2. Chapman, Hall. Dictionary of organic compounds; CRC press: New York, 1995.
3. A.R. Katritzky, M. Kuanar and S. Slavov, C.D. Hall, *Chem. Rev*. (2010) 5714–5789
4. B. Schmid and J. Gmehling, *J. Supercritical Fluids*. 55 (2010) 438–447
5. D. Frenkel and B. Smit, Understanding molecular simulation: From algorithm to applications; Academic Press: San Diego, 1996.
6. R. Gani and E.A. Brignole, *Fluid Phase Equilib*., 13 (1983) 331-340
7. J. Marrero and R. Gani, *Fluid Phase Equilib*.,183 (2001) 183–208.

A Computational Perspective on Non-Covalent Interactions and its Relevance to Separation Science

G. Narahari Sastry

Centre for Molecular Modeling, Indian Institute of Chemical Technology,
Hyderabad – 500 007, India.
gnsastry@iict.ac.in

Non-covalent interactions control the three dimensional structure of macromolecules and the way in which different molecules interact with each other. Atomic level understanding of condensed phase structure will aid our ability to develop understanding the factors which control the selectivity of one species over the other. In most cases of separation it is usually mediated by various non-covalent interactions. In our efforts to employ rigorous computations on the molecules of medium sizes which involve non-covalent interactions several interesting features were unraveled. In this talk we describe the studies on stacking interactions of buckybowls, the metal ion interactions in chemical and biological systems and the ion transport in the membrane proteins. The alkali and alkaline earth metal interactions in biological system is analyzed using computational methods and also through analyzing databases. The role, range and relevance of cation-π and $\pi-\pi$ interactions in determining the macromolecular structure will be explained. We also introduce how contrasting is the perspective of physicists and chemists in dealing with the non-covalent interactions. Further, we focus our attention on how a pair of non-covalent interactions mutually influences each others strength, through computational and structural analyses. The extent of cooperativity among the non-covalent interactions is analyzed and its effect on controlling the 3D-structure. In this talk, the relationship between separation science and understanding non-covalent interactions is delineated.

Coarse-grained molecular simulations of polymers and nanocomposites

Jayant K. Singh
Department of Chemical Engineering
IIT Kanpur
jayant@iitk.ac.in

Structure of polymers and nanoparticles in melts, blends or solutions can range from nanometer scale to microns or even larger. Similarly, the corresponding time scales of the dynamical processes relevant for different material properties span over a wide range, from femtoseconds to milliseconds, and even greater for large scale ordering processes such as phase separation, segregation and self-assembly. In this talk, I will describe the use of mesoscale simulations to address some of the important polymer problems such as DNA segregations using microchannels,phase diagram of nanoparticle dispersion in a polymer matrix, and rheology of polymer nanocomposites.

The dynamical properties of polymeric materials are greatly influenced by the presence of nanoparticles in them. Addition of nanoparticles in a polymer matrix changes the mechanical, rheological, and thermal properties of the composite material dramatically, which are largely due to the spatial organization of nanoparticles in the polymer matrix. The spatial distribution of nanoparticles in a polymer matrix largely depends on nanoparticle-polymer interaction. We demonstrate how entropy and enthalpy compete to generate different distribution of nanoparticles in a polymer matrix. The self-assembly of anisotropic nanoparticles has potential applications in optoelectronic and memory devices. However, the fabrication of such ordered structure is very sensitive to chemical and thermodynamics conditions. We demonstrate that the depletion force in a polymer solution could be used to generate the self-assembly of cubes and tetrahedrons into multidimensional structures. The size, shape and energy landscape of self-assembled structures of cubes and tetrahedrons in a polymer matrix are analyzed. We present phase diagrams, which show the spatial distributions of cubes and tetrahedrons in a polymer matrix for variable particle-polymer interaction and particles' volume fraction. Furthermore, the impact of nanoparticles on the rheology of polymer melt is also studied. We show that the viscosity of a polymer nanocomposite depends on the distribution of nanoparticles in it. The aggregation of nanoparticles in a polymer matrix leads to the decrease of the composite's viscosity.

REFERENCES

1. Ghosh A, Patra TK, Rishikant, Singh RK, Singh JK and Bhattacharya S, Surface Electrophoresis of ds-DNA across orthogonal pair of surfaces, *App. Phys. Lett.*98,164102 (2011)
2. Patra TK, Hens A and Singh JK, Vapor-liquid phase coexistence and transport properties of two-dimensional oligomers *J. Chem. Phys.* 137, 084701(2012)
3. Patra TK and Singh JK, Coarse-grain molecular dynamics simulations of nanoparticle-polymer melt: Dispersion vs. Agglomeration *J. Chem. Phys*. 138, 144901 (2013)
4. Patra TK and Singh JK, Polymer directed aggregation and dispersion of anisotropic nanoparticles *Soft Matter*,10, 1823 (2014)
5. Patra TK and Singh JK, Localization and Stretching of Polymer Chains at the Junction of two Surfaces *J. Chem. Phys*. 140, 204909 (2014)
6. Patra TK, Katiyar P and Singh JK. Substrate Directed Self-Assembly of Anisotropic Nanoparticles, *Chem. Eng. Sci.*121, 16 (2015)

Fluids in Nanochannels and Nanopores:As Envisaged through Molecular Dynamics Simulations

M. Chopra[1] and N. Choudhury[2]

[1]Radiation Safety Systems Division,
[2]Theoretical Chemistry Section, Chemistry Group,
Bhabha Atomic Research Centre, Mumbai-400 085, India.

Email: nihcho@barc.gov.in

Abstract. Transport of water through nanotubes and nanochannels is of fundamental as well as technological importance due to its relevance in biology, material science, chemistryand chemical engineering. Interplay of nano-confinement and inter-particle interactions makes the nanochannel-fluid system complex and intriguing. In the present work, based on our molecular dynamics simulation results, we shall discuss fundamental differences in structural and dynamical (transport) aspects of polar and nonpolar fluids when confined in or transported through carbon nanotubes. Current status of applicability of such nanochannels as gated channels or nano-filters will also be discussed.

Keywords: Flow through carbon nanotube, molecular dynamics simulation, translocation probability, conduction burst.

INTRODUCTION

Understanding behavior of fluids in nanochannels and nanopores is of fundamental as well as technological importance. Nanoconfinedfluid, because of its unusual properties that differ from those of bulk liquid and gaseous phases, has been the subject matter of intense research. Nanochannel-water system due to its wide applicability in nanofluidics, including electrophoretic and thermophoretic channels, membranes, sensors, filters, and gating devices, has been of prime technological importance. Central to many of these applications is the ability of these channels to transport fluids and other molecules with a molecular leveltunability and nanoscale precision. Atomistic molecular dynamics (MD) simulation, which has femtosecond temporal and Angstrom level spatial resolutions, is one of the most useful and valuable tool to investigate such a nanoscale system. Earlier pioneering investigation of CNT-water system using MD simulation has shown [1] many interesting features. Here we discuss various subtle issues relating to structural and dynamical (transport) aspects of polar and nonpolar fluids when confined in or transported through carbon nanotubes. Applicability of such nanochannels as gated channels or nano-filters will also be discussed.

MODEL AND SIMULATION DETAILS

Extensive molecular dynamics simulations have been carried out by using the AMBER96 force-filed parameters for sp^2 carbon atoms of the carbon nanotube (CNT), the Extended Simple Point Charge (SPC/E) model for water and the Optimized Potentials for Liquid Simulations-United Atom (OPLS-UA) model for methane.

RESULTS AND DISCUSSIONS

In Figure 1, normalized density of fluid in and around the CNT has been shown for methane as well as water. It is observed that packing of methane inside the CNT is more as compared to that of water. In order to get further insight, we have also shown instantaneous number of fluid molecules inside the CNT as a function of time. Despite its hydrophobic character, the nanotube channel remains occupied on an average with 5-6 water molecules or 3-4 methane molecules (Figure 2, top panel) during 20 ns simulation. Effect of solute-water van der Waals interaction has been investigated by reducing the solute-water interaction energy parameter ε. When $\varepsilon_{CO}$is reduced, transitions between filled (around 5 molecules) and empty (almost zero molecule) states are observed in case of water (Figure 2, left, bottom panel)but not in case of methane. Instead, the average number of methane molecules inside the CNT gradually decreases with the decrease in fluid-CNT interaction parameter ε_{CC4}(see Fig 2(b)all the panels).

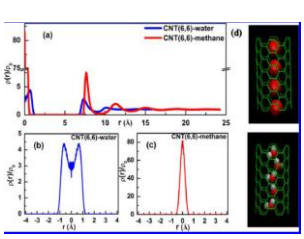

Figure 1. (a) Normalized density profile, $\rho(r)/\rho_0$, of fluids as a function of radial distance, r, measured from the center of the nanotube. The same for (b) water and (c) methane within CNT. (d) Snapshots of methane (upper panel) and zigzag orientation of water (lower panel) inside CNT.

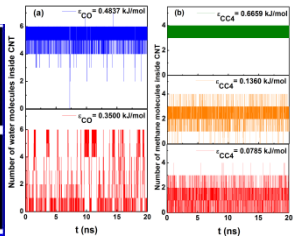

Figure 2. Number of fluid molecules inside the nanotube as a function of time for different carbon-fluid interactions for (a) CNT-water and (b) CNT-methane systems.

The pulse like transmission or the conduction burst (as shown by peaks in Figure 3) has been observed for both water and methane, showing this feature to be independent of polarity or hydrogen-bond forming ability of the fluid molecules [2-3]. It contradicts the explanation given by Hummer et. al. who attributed the conduction burst of water to the tight hydrogen-bonding network inside the nanotube [1]. If this is the case, then such a pulsed transmission should not have been observed in case of methane-CNT system. Hence, we conclude that the pulse-like conduction of fluid molecules does not have any relation with the polarity or hydrogen bond forming ability of the fluid molecules. It may be attributed to the single-file nature of the CNT-fluid system. The higher probability of translocation for methane (0.162) than that for water (0.092) indicates that the diffusivity of methane is higher than that of water.

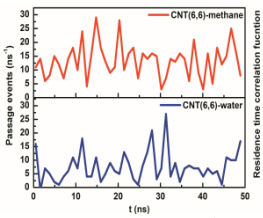

Figure 3. Number of translocate ion events of fluid molecules per nanosecond through the CNT. Conduction bursts as shown by the peaks have been observed in both the CNT-methane and the CNT-water systems.

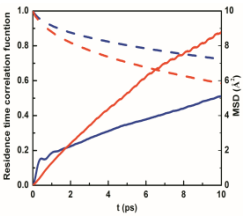

Figure 4. Residence time correlation function and MSD for water (blue curves) and methane (red curves) molecules inside the nanotube along the CNT axis (Residence time - dotted line, MSD - full line).

The diffusion constant along the axis of the CNT is obtained from the slope of a linear fit of the respective mean squared displacement (MSD) data calculated from simulation trajectory (Figure 4). The steeper slope of linear portion of the MSD curve for methane again indicates higher diffusivity of non-polar methane as compared to polar fluid (water) inside the CNT for the same CNT diameter.The residence time plots (not shown here) show the reverse trend, that is, the residence time of a molecule inside the CNT is higher for water than for methane and this trend is consistent with that of MSD results.Also the estimated lower activation energy for the diffusion and lower value of force due to CNT cage in case of methane as compared to that for water supports faster transport of methane molecules than that of water molecules through the nanotube [4].

Effect of many parameters such as wall charge, pressureetc. on the flow of ions and water through CNT [5] and graphene based artificial channels will be discussed.

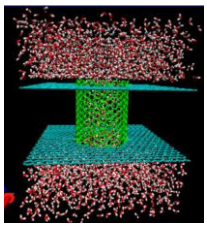

Figure 5. Snapshot of the simulation system, where the box size is about 5.1 × 5.1 × 6.1 nm^3. The two membrane sheets are charge neutral and the channel (green) is positively (or negatively) charged. The channel diameter and length are 2.02 and 2.56 nm, respectively.

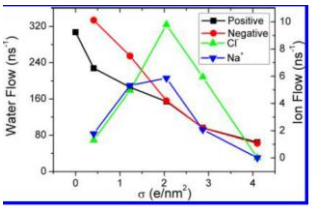

Figure 6. Water and ion flow as a function of the charge density forpositively and negatively charged channels, respectively. Error bars are shown for two data points and are smaller than the symbols.

ACKNOWLEDGEMENTS

It is a pleasure to thank Dr. B. N. Jagatap, Director, Chemistry Group for his kind interest and encouragement. Computer Division, BARC is gratefully acknowledged for providing AnupamSupercomputing Facility and support.

REFERENCES

1. G. Hummer, J. C. Rasaiah and J. P. Noworyta, Nature (London)414, 188-190 (2001); A. Berezhkovskii and G. Hummer, Phys. Rev. Lett. 89, 064503-1-4 (2002).

2. M. Chopra, R. Phatak and N. Choudhury, AIP Conf. Proc. 1512, 562-563 (2013).

3. M. Chopra and N. Choudhury, J. Phys. Chem. C 117, 18398−18405 (2013).

4. B. J. Borah, H. Jobic and S. Yashonath, J. Chem. Phys.132, 144507-1-11 (2010).

5. L. Hao, J. Su, H. Guo, J. Phys. Chem. B 117, 7685−7694 (2013)

A First Principles Approach to Materials Modeling: Implications towardH-Economy

C. Majumder
Chemistry Division, Bhabha Atomic Research Centre, Mumbai-400085
Email: chimaju@barc.gov.in

Abstract. The term "hydrogen economy" refers to the vision of using hydrogen as a low-carbon energy source – replacing, for example, gasoline as a transport fuel or natural gas as a heating fuel. This comprises of three primary steps; (i) production (ii) storage and (iii) transportation of hydrogen. Density functional theory in combination with molecular dynamics simulation approach has shown promising potential to model novel catalyst for these purposes. Here we present a brief summary of our recent works on the modeling of a catalyst for hydrogen production through S-I thermochemical route and hydrogen storage in C based materials.

Keywords: Hydrogen economy, DFT, Nanocatalysis

INTRODUCTION

Hydrogen is a fascinating energy carrier for clean environment. On reaction with oxygen, hydrogen forms water. This exothermic reaction yields 232 kJ/mol of water formed. The water is returned to nature where it originally came from. But hydrogen, the most common chemical element on the planet, does not exist in nature in its pure form. It has to be separated from chemical compounds, by electrolysis from water or by chemical processes from hydrocarbons or other hydrogen carriers. Both the production and the use of hydrogen have attracted highest attention during the past decade.

Density functional theory is an extremely successful approach for the description of ground state properties of metals, semiconductors, and insulators [1]. The success of density functional theory (DFT) not only encompasses standard bulk materials but also complex materials such as bio-molecules and nano-materials. In this article we provide an overview of the key concepts and recent developments in computational modelling of complex materials with a focus on applications in the field of catalytic materials.

COMPUTATIONAL APPROACH

All calculations have been carried out using the plane wave based pseudo-potential approach. While the total energy calculations were carried out under the DFT formalism, the geometrical search to locate the lowest energy structures has been carried out employing simulation tools [2].

RESULTS AND DISCUSSIONS

I. Modelling of Catalyst for Hydrogen Production:

Thermochemical cycles have the greatest prospect for hydrogen production from water in the large scale. The sulfur–iodine (S–I) thermochemical cycle for water splitting has attracted increasing attention because it can be efficiently used for mass scale production of hydrogen without CO_2 emissions. The decomposition of H_2SO_4 is the most energy demanding. In particular, the second part of the H_2SO_4 decomposition, where SO_3 is decomposed into SO_2 and O_2 requires very high temperature (between 750 and 900 °C) and does not occur without a catalyst.

With a view to design a novel-catalyst for SO_3 decomposition, we have investigated the interaction of SO_3 with supported noble metal clusters. The results showed that the interaction of the SO_3 molecule undergoes via metal–oxygen bond formation[3]. Other configurations with metal–sulfur connections are found to be higher in energy. It may be noted that the situation is different when we consider the interaction of SO_3 molecules with gas phase metal clusters, where Pd4 and Ag_2Pd_2 clusters bind with SO_3 through metal–sulfur bonds.Moreover, for both deposited and gas phase clusters, the elongation of the S–O bond is greater for the isomers where the SO_3 molecule is connected to the metal clusters through metal–oxygen bonds. For the interaction of SO_3 with $Ag_4@Al_2O_3$, $Pd_4@Al_2O_3$, and $Ag_2Pd_2@Al_2O_3$, it was found that the S–O bond elongates up to 1.52, 1.54, and 1.64 Å, respectively. We note that the S–O bond length of 1.64 Å is 14% more than the corresponding gas phase values. Further it is noticed that, for configurations with metal–oxygen bonds, the M–M bond of the M_4 cluster becomes longer or weaker than the situation where the SO_3 molecule connects through a metal–sulfur bond. A representative figure for the interaction of SO_3 with supported metal clusters is shown in figure 1.

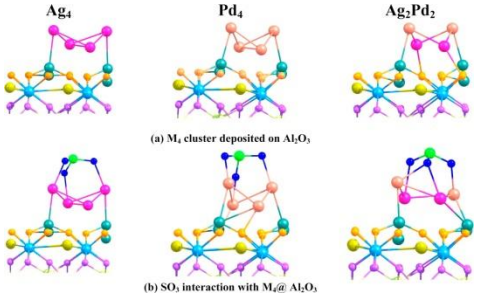

Fig.1*(a) Ground state geometries of M_4 cluster after deposition on Al_2O_3 surface. (b) Lowest energy structures of SO_3 molecule interacting with $M_4@Al_2O_3$ complex.*

Hydrogen Storage in C based or similar systems

The storage of hydrogen posesthe biggest challenge in a new hydrogen economy because thestorage medium must meet the requirements of high gravimetricand volumetric density, fast kinetics, and favorable thermodynamics [4].Magnesium-based systems are considered to be very promising hydrogen storage materials because of their low cost and high hydrogen storage capacity. With this motivation we have investigated the hydrogenation behavior of clean and doped Mg. The results suggest that the stabilization of Ni on the surface layer gives significant reduction in the dissociation barrier of thehydrogen molecule on the doped Mg surface [5].

We have also worked on the hydrogenation behaviour of C based nanomaterials [6]. It is seen that doping of nanotubes and layered sheets by transition metal atoms significantly enhance the storage capacity. Unlike transition metal decorated carbon fullerene, which suffers from the metal clustering, metallo-carbohedrenes (Met-Cars) are stable systems with transition metal atoms as part of the carbon nanostructures. The hydrogen storage properties of selected met-cars (M_8C_{12}, M = Sc, Ti, V) have been compared [7]. The results revealed that when the M = Ti, the cluster can take up total 16 hydrogen molecule by physisorption where the hydrogen molecules gets absorbed reversibly on the Ti atoms. The effective storagecapacity of the partially hydrogenated met-car with reversible adsorption-desorptionbehaviour is estimated to be 10.96 wt.% albeit total hydrogen loading capacity of 15.06wt.% foran isolated Ti_8C_{12} cluster. On the basis of the results, it is inferred that the partially hydrogenatedmet-cars are very promising high capacity reversible hydrogen storage materials.

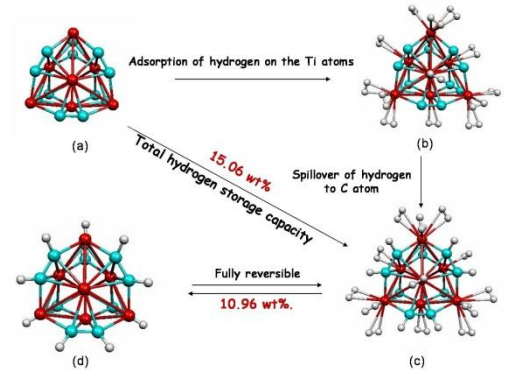

Fig. 5*A schematic representation of the hydrogen adsorption-desorption process in the Ti_8C_{12} cluster.*

Conclusion:

In summary, we have attempted to illustrate how DFT formalism can be utilized to develop a detailed molecular-level picture of catalytic materials. In particular, we have emphasized modelling of materials for use in the field of hydrogen economy. Through this brief review we have demonstrated that theoretical modelling provides new insight that can play a significant role in the design of advanced materials. Moreover, DFT opens exciting prospects for the discovery of new catalysts, a learned alternative to blind search. There is a long way to go before we have a general theoretical description of heterogeneous catalysis. Catalysts are complicated, multiphase materials, and there are an enormous number of interesting catalytic processes. We are just at the beginning of an era where DFT calculations contribute a new perspective to the many important experimental tools that have been developed to understand surface reactivity.

ACKNOWLEDGEMENTS

Computer Division, BARC, is gratefully acknowledged for providing the Anupam parallel computational facility.

REFERENCES

1. P. Hohenburg and W. Kohn, *Phys. Rev.* **136** B864 (1964); W. Kohn and L. J. Sham, *Phys. Rev.* **140** A1133 (1965).
2. G. Kresse, J. Furthmu¨ller, VASP the Guide. Available from http://cms.mip.univie.ac.at/VASP.; M.C. Payne, M.P. Teter, D.C. Allan, T.A. Arias, J.D. Joannopoulos Rev. Modern Phys., 64 (1992), pp. 1046–1097.
3. S. Nigam, C. Majumder, *Int. J Hydrogen Energy*,*37*, 3645-3651**(2012);**S. Nigam, C. Majumder, *Chem. Phys. Lett.*,*537*, 69-74**(2012);** S. Nigam, C. Majumder, *J. Phys. Chem. C*,*116*,25594(2012).
4. A. Zuttel, P. Sudan, Ph. Mauron, T. Kiyobayashi, Ch. Emmenegger, L. Schlabach. *Int J Hydrogen Energy***27** 203 (2002).
5. S. Banerjee, C. G. S. Pillai, and C. Majumder, *Journal of Chemical Physics***129** 174703 (2008); Seemita Banerjee, C. G. S. Pillai, and C. Majumder, *Journal of Physical Chemistry C***113** 10574, (2009).
6. S. Bhattacharya, C. Majumder, G. P. Das, *Journal of Physical Chemistry C*, **112**, 17487 (2008); S. Banerjee, C. G. S. Pillai, C. Majumder, *Int J Hydrogen Energy***35** 2344, (2010); S. Banerjee, S. Nigam, C. G. S. Pillai, C. Majumder, *Int J Hydrogen Energy*, **37** 3733, (2012);A.Bhattacharya, S.Bhattacharya, C.Majumder and G.P.Das, J. Phys. Chem. C. 114 (2010) 10297-10301;S. Banerjee, C. G. S. Pillai, C. Majumder, *Int J Hydrogen Energy***36** 4976, (2011).
7. S. Banerjee, C. G. S. Pillai, C. Majumder, *Applied Physics Letters*, **102** 073901 (2013).

Unusual Dynamical Features of Hydrocarbons Adsorbed in Porous Media: MD Simulation Study

S. Mitra, V.K. Sharma, S.A. Prabhudesai and R. Mukhopadhyay
Solid State Physics Division, Physics Group
Bhabha Atomic Research Centre, Mumbai-400085

Email: smitra@barc.gov.in

Abstract. Detailed dynamical landscapes of propylene adsorbed in ZSM5 and Na–Y zeolites and acetylene adsorbed in CuBTC metal organic framework (MOF) as studied by molecular dynamics (MD) simulation are discussed here. Zeolites represent a class of technologically important materials because of their characteristic properties of molecular sieving and catalysis, which makes them indispensable in the petroleum industries, while MOF has demonstrated remarkable storage capabilities for hydrocarbons at atmospheric pressure. Aim of these studies is to investigate the correlation of the host topology towards the diffusion of guest molecules. Several unusual dynamical features of guest hydrocarbons inside the porous host structures have been explained on the basis of MD simulation results which shed light on the complex diffusion processes of guest molecules inside porous host matrices.

Keywords: Diffusion, Zeolite, Metal Organic Framework, Molecular Dynamics Simulation

INTRODUCTION

The problem of diffusion of molecules in confined geometries can be found in a large variety of physical situations. Common examples that impose spatial restriction include zeolites, metal organic frameworks, clays, etc. Confinement appears in variety of phenomena, starting from the case where atoms, molecules, liquids or solids are enclosed in 3-dimensional pores, to cases where atoms or molecules are restricted within a 2 dimensional space, like in variety of clays, thin films or at surfaces. Experimentally, a significant change of the properties due to spatial restriction vis-à-vis their bulk is now well established [1]. Nevertheless, the influence of the confining materials e.g., the geometry of pores and the role of the interaction with interfaces are yet to be understood in detail. Zeolites and metal organic frameworks (MOFs) have attracted a great deal of attention during recent years because of their high specific pore volume, which opens up prospective applications such as gas storage, heterogeneous catalysis, gas separation, and purification. While these properties depend upon many factors including the acidity and the temperature stability of these porous materials, dynamics of guest molecules also play a major role. In order to be able to tailor make these materials for use in industry, it is important to understand the dynamical properties of guest molecules adsorbed in these porous materials. The results of our molecular dynamics (MD) simulation studies on propylene adsorbed in Na-Y and ZSM5 zeolite and acetylene adsorbed in MOF showed some unusual dynamical behaviour of guest molecules which are discussed here.

ZEOLITE AND MOF

ZSM5 and Na–Y are the two zeolitic systems in which the dynamics of adsorbed hydrocarbons have been studied quite extensively. ZSM5 zeolite is typified by a network of intersecting channels. In ZSM5 zeolite there are straight channels with an elliptical cross section of approximately 5.7–5.2 Å and parallel to the crystallographic axis *b*. The sinusoidal channels are nearly circular cross section of 5.4 Å in the *a*–*c* plane. Na–Y zeolite has a network of almost spherical supercages (surrounded by sodalite cages connected on their hexagonal faces), which are interconnected with each other in a tetrahedral manner by 12 membered oxygen rings forming windows. The diameter of these windows is about 7.8 Å while the supercages have a diameter of 11.8 Å.

Copper 1, 3, 5-benzenetricarboxylate (CuBTC) MOF consists of the metal corners of the Cu^{2+} ions coordinated to each other with benzene 1, 3, 5 tricarboxylate (BTC) organic ligands. Its structure exhibits a complex trimodal pore distribution [3], with a topology resulting in connectivity between some but not all of the pores. Out of three different types of pores, one is relatively small in size (~5 Å) and like side pockets of tetrahedral-shape. The other two are comparatively large pores and can be designated as L1 and L2. Pore L1 is cuboctahedral and approximately 10.7 Å across. Pore L1 is connected via square window to a secondary pore

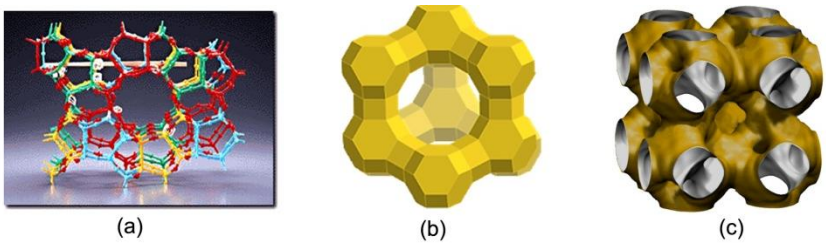

Fig. 1 Schematic of (a) ZSM5 zeolite and (b) Na–Y zeolite and (c) CuBTC metal organic framework

system (pore L2), size of which is ~ 12.7 Å. Pore L2 is connected to the tetrahedral pockets via triangular windows. Schematic of Na-Y and ZSM5 zeolite and CuBTC MOF are shown in Fig. 1.

MD SIMULATION

MD simulation of propylene molecules confined in ZSM5 and Na–Y zeolite and acetylene molecules adsorbed in CuBTC MOF have been carried out in micro-canonical ensemble. Atomic positions of ZSM5, Na–Y zeolite and CuBTC MOF are taken from the work reported by Koningsveld et al. [3], Fitch et al. [4] and Peterson et al. [2] respectively. Atomic positions of propylene and acetylene molecules are considered as rigid molecules and therefore the bond angle and bond lengths between the sites are kept constant throughout the simulation. Intermolecular interactions were modelled by Lennard–Jones (6–12) potential [5]. An all-atom model was used for propylene, i.e., the hydrogen-atom interactions are taken explicitly. Acetylene molecule is modelled as two interacting sites under united atom model. MD simulations are carried out for three different concentrations (4, 10 and 14 molecules) of acetylene molecules per unit cell of CuBTC MOF. Eight propylene molecules per unit cell of ZSM5 zeolite and 3 propylene molecules per Na-Y supercage are used for the simulation.

RESULTS AND DISCUSSION

Translational motion of any molecule can be monitored from the center of mass (COM) trajectories obtained from MD simulation. Diffusion constants estimated from the slope of the COM mean square displacement (MSD) curves are found to be 5.4×10^{-5} cm^2/sec and 1.0×10^{-5} cm^2/sec in case of Na–Y and ZSM5 respectively. This is a clear manifestation of the effect of topology of the host zeolites since the restriction imposed by the channel structure of the ZSM5 on propylene molecules is much more than that by Na-Y zeolite. Intermediate scattering functions corresponding to translational motion revealed that it consists of three components with different time scales. At short time and small length scales, a molecule does not interact with other molecules and therefore acts as a free particle (ideal gas). In case of zeolite, dynamics is determined by its pore topology and it is found that at long time and large length scales, dynamics is occurring in two different time scales. On the other hand, rotational dynamics of propylene adsorbed in ZSM5 is found to be anisotropic in nature as the molecule does not have full freedom to rotate in all directions in a particular channel. However, at sufficiently long time, the molecule can diffuse to another channel and so cover all the different orientations. This is in contrast to Na–Y zeolite where the large size of the host cages leaves the isotropic rotation of propylene unhindered even at short times. It is also found that the propylene molecules prefer its orientation along the channel direction during diffusion through the ZSM5 zeolitic channels unlike that in Na–Y zeolite [5].

MD simulation study has revealed interesting results towards dynamical pathways of acetylene in the complex structure of CuBTC metal organic framework. Diffusivity of acetylene molecules inside CuBTC MOF is found to increase with concentration which has been explained on the basis of the trajectories and the free energy map. At low concentration, most of the molecules are found to be trapped in the tetrahedral pockets whereas at high concentration relative population in the large pore increases and more number of molecules diffuse through the large pores. Since the acetylene molecules experience less energy barrier while passing through large pores, the average diffusivity increases at higher concentration. It was concluded that the pathways followed by the guest molecules decide diffusion process within CuBTC framework [6].

REFERENCES

1. D.R. Cole, E. Mamontov, G. Rother, L. Liang, R. Rinaldi, H. Schober (Eds.), *Neutron Applications in Earth, Energy and Environmental Sciences*, Springer-Verlag, Berlin, 2009 (Chapter 19), p. 547.
2. V.K. Peterson, C.M. Brown, Y. Liu, C.J. Kepert, *J. Phys. Chem. C* **115**, 8851 (2011).
3. H. Van Koningsveld, H. Van Bekkum, J.C. Jansen, *Acta. Cryst. B* **43** 127 (1987).
4. A.N. Fitch, H. Jobic, A. Renouprez, *J. Phys. Chem.* **90,** 1311 (1986).
5. S. Mitra, V.K. Sharma, S.L. Chaplot, R. Mukhopadhyay, Chem. Phys. **430**, 69 (2014).
6. S.A. Prabhudesai, V.K. Sharma, S. Mitra, and R. Mukhopadhyay, *Eur. Phys. J. B* **86**: 145 (2013)

Dynamical Correlations and Negative Maxwell–Stefan Diffusivities for molten salt LiCl-KCl and LiF-BeF2

Brahmananda Chakraborty[1], Dane Morgan[2], Jacob Eapen[3]
[1]High Pressure & Synchrotron Radiation Physics Division, Bhabha Atomic Research Centre, Mumbai-400085
[2] University of Wisconsin, Madison, USA, 3North Carolina State University, USA.

Email: brahma@barc.gov.in

Abstract. Multicomponent diffusional mechanisms in ternary systems LiCl-KCl and LiF-BeF2 are elucidated using the Green–Kubo formalism. We observe a sign change and a divergent–like behavior for the MS diffusivity of the K–Li ion pair at a temperature of 1095K for the eutectic composition, and at a KCl mole fraction of 0.48 at 1043K. For molten coolant LiF-BeF2 MS diffusivity shows strong composition dependence with negative MS diffusivity even between positive-negative pairs for low LiF%. Negative MS diffusivities while unusual are however, shown to satisfy the non-negative entropic constraints. Local structure of solutes Sr and U in LiCl-KCl make more bonds with Cl ions for higher oxidation states and the first peak radial distribution function is greater.

Keywords: Molten salt, Nuclear Waste Separation, Coolant, LiCl-KCl, Flibe, MS Diffusivity

INTRODUCTION

The separation of actinides and fission products is a central step in closing the nuclear fuel cycle. In the pyrometallurgical recycling process, the spent nuclear fuel is dissolved in a molten salt such as LiCl and/or KCl followed by the extraction of actinides by electrorefining and/or electroreduction processes [1, 2]. Knowledge of a number of basic thermokinetic properties of salts and salt-fuel mixtures is necessary for optimizing present and developing new approaches for pyrometallurgical waste processing.

Molten salt LiF-BeF2 is a potential candidate for coolant in High Temperature Reactor [3].The structure and dynamics of the molten salt at operating temperature and pressure has impact on the performance of the reactor. Considering the importance of LiCl-KCl and LiF-BeF2 in nuclear industry, here we present the dynamical correlations and Maxwell-Stefan (MS) diffusivity for LiCl-KCl and LiF-BeF_2 at various temperature and composition. Local structure of various actinides Sr, La and U ions in the LiCl-KCl molten salts were also studied.

THEORY

In the MS framework, the driving force for diffusion of component *i* is balanced by the frictional force bewteen the component *i* and other components [4]

where MS diffusivity $Đ_{ij}$ has the physical significance of an inverse drag force. The Onsager coefficients (Λ_{ik}) are evaluated from the linear response theory using equilibrium MD simulations in barycentric referrence frame [10] given by

$$\Lambda_{ik}^{0} = \frac{1}{3N}\int_{0}^{\infty} dt \left\langle \Im_i^0(t)\Im_k^0(0)\right\rangle \equiv \frac{1}{3N}\int_{0}^{\infty} dt \Psi_{ik}^{0}(t)$$

where N is the total number of atoms/ions and $\Psi(t)$ denotes the ensemble average of the diffusive mass flux correlation.The volume averaged diffusive flux is given by

$$\Im_k^0(t) = \int_{\Omega} \mathbf{j}_k(\mathbf{r},t) = \sum_{l=1}^{N_k}\left[\mathbf{u}_k^l(t) - \mathbf{V}^0(t)\right]$$

And finally, the MS diffusivities can be expressed as

$$Đ_{12} = \left[B_{11} - \left(1+\frac{x_3}{x_1}\right)B_{12}\right]^{-1}$$

$$Đ_{23} = \left[B_{22} + \left(\frac{x_1}{x_2}\right)B_{21}\right]^{-1}$$

$$Đ_{13} = \left[B_{11} + \left(\frac{x_2}{x_1}\right)B_{12}\right]^{-1}$$

Where x_i, are the mole fraction and B matrix is obtained from Λ_{ik} [5].

COMPUTATIONAL PROTOCOL

To compute the Onsager phenomenological coefficients for ternary systems we have developed various modules

using and incorporated these modules to MD code DL_POLY_4 [6]. MD simulations are performed in a cubic cell with periodic boundary conditions where the ions interact through a long–ranged electrostatic potential and a Born–Mayer–Huggins (BHM) short–ranged potential, originally developed by Fumi and Tosi [7].

RESULTS AND DISCUSSIONS

Fig. 1 delineates the variation of MS diffusivities for LiCl-KCl with temperature at eutectic composition.Interestingly we observe negative and divergent MS diffusivity between the positive-positive ion pair Li-K. At eutectic mixture the MS diffusivity between ion pair Li-K diverges at around 1095 K.

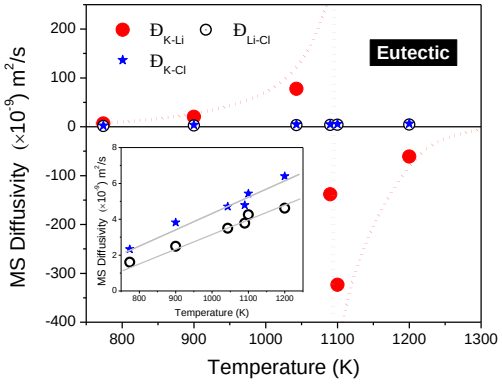

FIGURE 1. MS diffusivities for different temperatures at eutectic composition. (Inset) $Đ_{Li-Cl}$ and $Đ_{K-Cl}$ on a magnified scale.

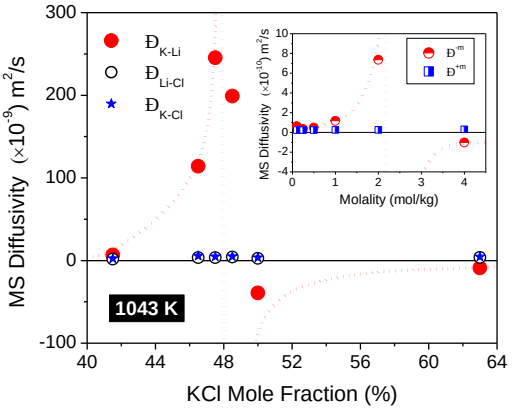

FIGURE 2. MS diffusivities for different compositions at 1043K. (Inset) Experimental MS diffusivities in an ion exchange membrane [5].

In Fig. 2 we show the MS diffusivities as a function of composition at 1043K. As observed with the variation for temperature, the MS diffusivity for the K–Li ion pair tends to portray a diverging behavior at a KCl mole fraction of 0.48, approximately. The variation of $Đ_{K-Li}$ strikingly similar to those observed in experiments; the inset shows a MS diffusivity data set for like–like ions in an exchange membrane system [5]. We have verified that negative and diverging MS diffusivity satisfies the non-negative entropy production rate governed by 2nd law of thermodynamics [4]. Fig. 3 shows the strong composition dependence of MS diffusivity for LiF-BeF2 where the MS diffusivity between the positive-negative pair also becomes negative at small mole fraction of LiF. Local structures of Sr and U solutes in Licl-KCl are presteed in Fig. 4. When solute has higher oxidation states, it will make more bonds with Cl ions and the first peak is of radial distribution function is greater.

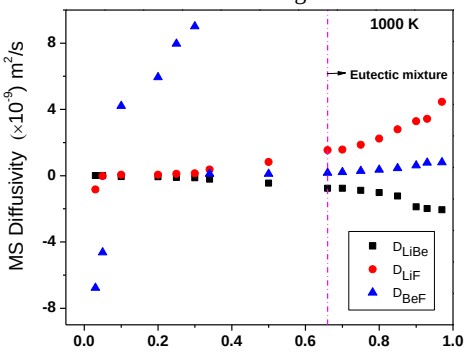

FIGURE 3. MS diffusivities of LiF-BeF2 for different compositions at 1000K.

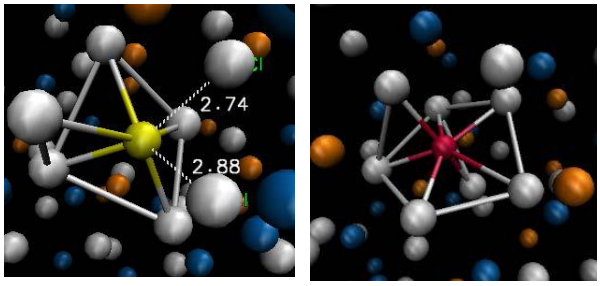

FIGURE 4. Local structures of Sr and U solutes in Licl-KCl with $SrCl_2$ and UCl_3

REFERENCES

1. Y. Sakamura, et al., J. Nucl. Sci. Tech. 35, 49 (1998).
2. T. Kato, T. Inoue, T. Iwai, and Y. Arai, J. Nucl. Mater. 357, 105 (2006).
3. W.R. Grimes, *Nucl. Appl. Technol.*, **8**, 137 (1970).
4. R. Krishna, and J. A. Wesselingh, *Chem. Eng. Sci.* **52**, 861 (1997).
5. B. Chakraborty, J. Wang and J. Eapen, *Phys. Rev. E* **87**, 052312 (2013).
6. I. T. Todorov, and W. Smith, *Phil. Trans. R. Soc. Lond.* A **362**, 1835 (2004).
7. M. P. Tosi, and F. G. Fumi, J. *Phys. Chem. Solids* **25**, 45 (1964).

DFT Modeling on Functionalized Carbon Nanomaterials for Adsorptive Separation of Metal Ions

A.K. Singha Deb, Sk. M. Ali, K.T. Shenoy
Chemical Engineering Division,
Bhabha Atomic Research Centre, Mumbai-400085
Homi Bhabha National Institute

Email: aksdeb@barc.gov.in

Abstract. Carbon nanotubes (CNT) and fullerenes (e.g. C60) are the carbon nanomaterials (CNMs) that have recently attracted the attention of scientists and technologists for their applications in diverse field owing to their unique physical and chemical properties. Functionalized CNMs have been shown to be more sensitive and selective for removal of inorganic and organics from aqueous medium compared to pristine one. DFT calculation that carried out for Th^{4+} binding with carboxylic acid functionalized CNT and C60 in gas and aqueous phase showed that former has higher adsorption than the later. From DFT aided energetic and thermodynamic calculations it was seen that the crown ether (benzo-15-crown-5, B15C5) functionalized CNT extracts Na^+ more preferentially than other alkali metal ions (Li^+, K^+), whereas batch adsorption studies show that B15C5-CNT have no adsorption for Li^+ and higher adsorption for K^+ over Na^+. Theoretically guided modeling of various functionalized CNMs along with experimental verification will lead to development of super nanoadsorbent for environmental application.

Keywords: DFT modeling, Carbon nanomaterials, Functionalization, actinide adsorption, alkali metals adsorption

INTRODUCTION

Amongst other carbon nanomaterials (CNMs), carbon nanotubes and fullerenes have been coming out as efficient sorbent material for environmental application as they have sorbent friendly properties like large surface area, porous network layered structures along with their decreasing production cost with the time [1, 2]. CNMs in pristine form lacks in sensitivity and selectivity for a particular metal ion/organic matter adsorption. The selectivity of CNMs can be grown by introducing appropriate functional groups on the surface, by covalent of non-covalent means [3].

DFT modeling can model the energetic and thermodynamic parameter of adsorption after optimizing the structures of the CNMs and functionalized CNMs molecules and their metal ion complexes using quantum mechanical calculations with proper basis set and functional.

Carboxylic acid functional groups (-COOH) are well known for their strong binding interaction with various metal ions of environmental, catalytic and biological importance. Crown ethers have unique ability to selectively chelate alkali metal ions from solutions.

Selective separation of thorium from aqueous solution is important as it acts as an alternate fuel of future nuclear reactor and its presence in living organism is deleterious. The lithium which is used for various applications in nuclear and aeronautical industry must be in suitable state of purity and in particular it must contain very little alkali metals such as sodium and potassium as these elements downgrade the performances of lithium.

In this article, DFT calculations was performed for the Th^{4+} binding with carboxylic acid functionalized CNTs (CNT-COOH) and C60 fullerene (C60-COOH). The computed extent of adsorption values by these CNMs were compared with available experimental values. DFT aided energetic and thermodynamic calculations were carried out for the interaction of alkali metals (Li^+, Na^+ and Cs^+) ions with crown ether (B15C5) functionalized CNTs. The calculated trend in energy of interaction was verified with the experimentally obtained adsorption capacity values of synthesized B15C5-CNTs for alkali metal uptake.

COMPUTATIONAL DETAILS

All the geometries of the free as well complexes are optimized using Turbomole [4] package at BP86/SVP level of theory [5]. Single point energy calculations were carried out on optimized complexes at B3LYP/TZVP [6] level of theory. The zero point energy and thermodynamic correction to the total energy were made to compute the free energy at T=298.15K. The solvent effect in the energetic was incorporated employing conductor line screening model (COSMO) [7].

METHODS

The complexation ability of functionalized CNMs with metal ions can be evaluated from the gas phase binding energy (BE). The BE (ΔE) of the metal ion (M^{n+}) and CNTs (L) complexation reaction,

$$M^{n+} + L = M^{n+}L \qquad (1)$$

is defined by the following general relation,

$$\Delta E = E_{M^{n+}-CNM} - (E_{M^{n+}} + E_{CNM}) \qquad (2)$$

where, $E_{M^{n+}-CNM}$, $E_{M^{n+}}$ and E_{CNM} refer to the energy of M^{n+}-CNM complex, M^{n+} ion and the free CNM system respectively.

The thermal correction to the electronic energy (E_{el}), enthalpy (H) and free energy (G) of the optimized structures has been performed to predict the thermodynamic parameters[41]. The thermal and zero point energy corrected binding energy is

$$\Delta U = U_{M^{n+}-CNM} - (U_{M^{n+}} + U_{CNM}) \qquad (3)$$

where , $U_{M^{n+}-CNM}$, $U_{M^{n+}}$ and U_{CNM} represent the internal energy of the M^{n+} -CNM complex, M^{n+} ion and the free CNM system respectively.

The binding enthalpy (ΔH) and binding free energy (ΔG) for the metal ion-CNT complexation reaction in Eq. (1) are calculated using the following standard thermodynamic relations

$$\Delta H = \Delta U + \Delta nRT \qquad (4)$$

$$\Delta G = \Delta H - T\Delta S \qquad (5)$$

RESULTS AND DISCUSSIONS

Th^{4+} adsorption on CNM-COOH: The CNT considered here is a (8, 0) zigzag single-walled CNT which consists of four unit cells with tubular length of 5.78 Å width of 6.40 Å [8]. The fullerene unit consist of sixty carbon atoms with twenty hexagons and twelve pentagons.

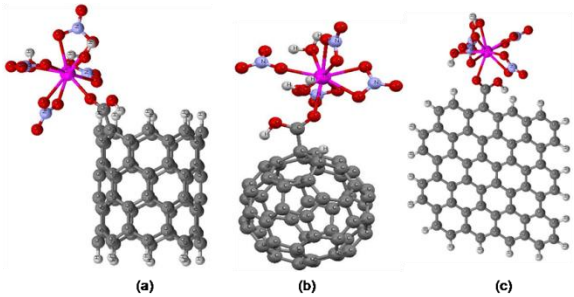

Fig. 1. Optimized structures of Th complexes with -COOH functionalized (a) CNT, (b) C60 and (c) Graphene.

We have considered one -COOH on the surface of CNT and C60. For CNT, the carboxyl group has been attached to the open edge carbon atoms (with dangling bonds) of the tube and for C60, one double bond has been substituted with one carboxyl and one hydrogen. Thorium in tetravalent state has been complexed with each of the -COOH functionalized CNMs, first, in absence and then, in presence of nitrate and water molecules. The optimized geometries of Th complexes with CNT-COOH and C60-COOH in presence of nitrate and aqua co-ligands and the calculated structural parameters are displayed in Fig. 1 and Table 1, respectively. In the optimized structures, the C-C and C-H bond distance of both CNT and C60 unit was found to be 1.44Å and 1.11Å which confirms the sp^2 carbon network. This is also same for optimized structure of Th complex of graphene-COOH (Fig 1c). The Th-O distance with nitrate ion is smaller than that of water molecule. It is also clear from Table1 that CNT-COOH form stronger complex with thorium compared to C60-COOH as the carbonyl oxygen to metal distance is shorter for the former. That carboxyl group of CNT binds more strongly to Th than that of C60 is also evident from the more C=O distances of the former; due to the strong interaction of donor O to metal ion, C=O bond weakened. This also is supported by the electronic and and thermodynamic energy parameters values of the interaction shown in Table 3. The binding energy (ΔE) of CNT-COOH is higher than C60-COOH by 22 kcal/mol. The free energy of Th adsorption by CNT-COOH both in gas and solvent phase was found to be higher than that of C60-COOH. Hence, it can be concluded that CNT-COOH is more efficient Th adsorbent than C60-COOH.

Table 1. Calculated structural parameters (in Å) of Th^{4+} ion with COOH functionalized CNT, C60 and G at BP/SVP level of theory.

System	$d_{M-O(=C)}$	$d_{C=O}$	$d_{M-O(NO3)}$	$d_{M-O(H2O)}$
CNT-COOH	2.36 Å	1.27 Å	2.50 Å	2.55 Å
C60-COOH	2.58 Å	1.23 Å	2.45 Å	2.57 Å

Table 2. Electronic and thermodynamic energies (in kcal/mol) of Th^{4+} ion with COOH functionalized CNMs in presence of nitrate ion and aqua molecules at B3LYP/TZVP level of theory.

Th complex system with	ΔE	ΔG_{gas}	ΔG_{sol}
CNT-COOH	-922.38	-930.29	-65.80
C60-COOH	-910.59	-919.46	-49.99

Alkali metal adsorption on CNT-B15C5: The CNT-COOH of the above work was attached to aminobenzo-15C5 with amide linkage. The optimized structure of the complexes of CNT-B15C5 with Li^+, Na^+ and K^+ ions are displayed in Fig. 2. It is seen that the Li^+ ion is situated at the centre of the crown ring between five O atoms, whereas the Na^+ and K^+ are situated outside of the cavity of the ring. The K^+ is more outward than the Na^+. From the Table 4, it is seen that the free energy of adsorption is high for Na^+ and K^+ ion, whereas, for Li^+ ion it is positive indication the high selectivity of Na^+ and K^+ ions over Li^+ ion. The computed selectivity was validated by performing the experiments as follows.

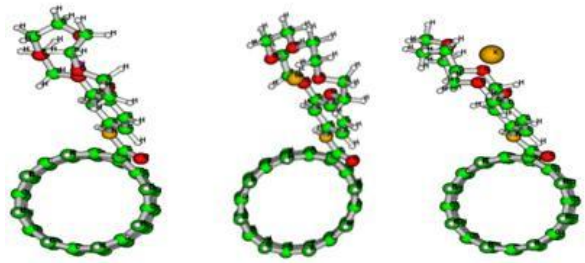

Fig. 2. optimized structures of CNT-B15C5 complexes with Li^+, Na^+ and K^+.

Table 4. Calculated energy parameters (in kcal/mol) of B15C5-CNT-metal ion in aqueous phase using B3LYP level of theory.

System	Li	Na	K
ΔU	-11.97	-22.10	-13.64
ΔH	-12.56	-22.69	-14.23
ΔS*	-0.05	-0.02	-0.03
ΔG	2.37	-14.35	-3.93
Exptl. q_e (mg/g)	-	19.95	63.62

*(kcal/mol/K)

B15C5-CNT was synthesized in laboratory by coupling amidation reaction between aminobenzo-15C5 and carboxyl-multiwalled-CNTs in presence of N, N'-dicyclohexylcarbodiimide (DCC) as coupling agent and dimethylaminopyridine (DMAP) as catalyst. The adsorption capacity, q_e ,values of K^+ is more than Na^+ or Li^+ implying that B15C5-CNT show more selectivity toward K^+ ion than Na^+. From the experimental results it can also be seen that Li^+ ion shows no extraction with B15C5-CNT. This means that working Li^+ solution (which always have other alkali metals, Na^+ and K^+, as impurities), CNT-B15C5 can remove the other ions except the Li^+ resulting in purifying the Li content. The mismatch of the uptake order of Na^+ and K^+ by B15C5-CNT between theory and experimental study needs further investigation.

Acknowledgement
Computer division BARC is acknowledged for providing ANUPAM supercomputing facility.

REFERENCES

1. Mauter, M. S.; Elimelech M., Environmental applications of carbon-based nanomaterials. Environ. Sci. Technol. 2008, 42, 5843-5859.
2. X. Ren, C. Chen, M. Nagatsu, X. Wang, Carbon nanotubes as adsorbents in environmental pollution management: A review, Chem. Eng. J., 2011, **170**, 395.
3. Maiti, U. N.; Lee, W. J.; Lee J. M.; Oh, Y.; Kim, J. Y.; Eim, J. E.; Shim, J.; Han, T. H.; Kim, S. O., 25th Anniversary Article: Chemically Modified/Doped Carbon Nanotubes & Graphene for Optimized Nanostructures & Nanodevices, Adv. Mater. **2014**, 26, 40–67.
4. Ahlrichs, R.; Bar, M.; Haser, M.; Horn, H.; Kolmel, C. Electronic structure calculations on workstation computers: The program system turbomole. Chem. Phys. Lett. **1989**, 162, 165-169.
5. Schaefer, A.; Horn, H.; Ahlrichs, R. J. Fully optimized contracted Gaussian basis sets for atoms Li to Kr. J. Chem. Phys. **1992**, 97, 2751–2777.
6. Becke, A.D. Density-functional thermochemistry. III. The role of exact exchange. J. Chem. Phys. **1993**, 98, 5648-5652; Lee, C.; Wang, W.; Parr, R. G. Development of the Colle-Salvetti correlation-energy formula into a functional of the electron density. Phys. Rev. B: Condens. Matter, 1988, 37, 785-789.
7. Klamt, A. Conductor-like screening model for real solvents: A new approach to the quantitative calculation of solvation phenomena. J. Phys. Chem. **1995**, 99, 2224-2235.
8. Singha Deb, A. K.; Ali, S. M.; Shenoy, K. T., Ghosh, S. K.; Adsorption of Eu3+ and Am3+ ion towards hard donor-based diglycolamic acid-functionalised carbon nanotubes: density functional theory guided experimental verification, Molecular Simulation **2014**, DOI: 10.1080/08927022.2014.977891.

Editors

K.T. Shenoy

Sk. M. Ali

A. Boda

A.K. Singha Deb

P.Sahu